Fnip1 Regulates Skeletal Muscle Fiber Type Specification, Fatigue Resistance, and Susceptibility to Muscular Dystrophy

Nicholas L. Reyes

A thesis
submitted in partial fulfillment of the
requirements for the degree of

Master of Science
University of Washington
2014

Committee:
Brian M. Iritani
Lillian Maggio-Price
Denny Liggitt

Program Authorized to Offer Degree:
The Department of Comparative Medicine

University of Washington

Abstract

Fnip1 Regulates Skeletal Muscle Fiber Type Specification, Fatigue Resistance, and Susceptibility to Muscular Dystrophy

Nicholas L. Reyes

Chair of the Supervisory Committee:
Brian M. Iritani, DVM PhD
Department of Comparative Medicine

Skeletal muscle is characterized by the presence of two distinct categories of muscle fibers called Type I "red" slow twitch and Type II "white" fast twitch, which display marked differences in contraction strength, metabolic strategies, and susceptibility to fatigue. The relative representation of each fiber type can have major influences on the susceptibility to metabolic diseases including obesity, diabetes, and muscular dystrophies. However, the molecular factors controlling fiber type specification remain poorly defined. The objective of my thesis was to investigate the roles of a new metabolic protein called Folliculin Interacting Protein-1 (Fnip1) in fiber type specification and susceptibility to metabolic disease. Utilizing *Fnip1* null mice we previously generated, we found that loss of Fnip1 dramatically increased the representation of Type I slow twitch fibers characterized by increased Myoglobin, MyH7, Succinate dehydrogenase (SDH) , Troponin I 1, Troponin C1, Troponin T1, and massive increases in mitochondria. Cultured *Fnip1* null muscle fibers had higher oxidative capacity, and isolated *Fnip1* null skeletal muscles sustained moı prolonged contraction and had more rapid post-contraction recovery when compared to wild-type skeletal muscle. Biochemical and molecular analyses revealed increased activation of the metabolic sensor AMP kinase and increased expression of the master

metabolic transcriptional regulator PGC1α. Genetic disruption of PGC1α rescued normal levels of Type I fibers markers in *Fnip1*-null mice. Remarkably, loss of Fnip1 nearly completely prevented muscle damage in a murine model of Duchenne muscular dystrophy. These results indicate that Fnip1 controls skeletal muscle fiber type specification, and suggest that inhibition of Fnip1 could be used as a potential therapeutic strategy to increase mitochondrial biogenesis and muscle function in patients with muscular dystrophy diseases, which are typified by defective mitochondrial function.

Table of Contents

List of Figures

Acronyms and Abbreviations

4EBP1- Eukaryotic Translation Initiation Factor 4E-Binding Protein 1
ACC-Acetyl CoA Carboxylase
AKT- Protein Kinase B
AMPK- AMP activated protein kinase
ATP5γ1- ATP Synthase
BHD- Birt-Hogg-Dube' Syndrome
CaMK-Calmodulin Kinase
CK-Creatine Kinase
Cytb- Cytochrome B
Cyto C- Cytochrome C
DAPI- 4',6-diamidino-2-phenylindole
DMD- Duschenne's Muscular Dystrophy
EBD- Evan's Blue Dye
ECAR- Exreacellular Acidification Rate
EDL- *Extensor Digitalis Longus*
EIF4E-Eukaryotic Translation Initiation Factor 4E
EM- Electron Microscopy
ENU-N-ethyl-N-nitrosourea
ERRα-Estrogen-Related Receptor Alpha
FCLN- Folliculin
Fnip1- Folliculin Interacting Protein 1
Fnip2- Folliculin Interacting Protein 2
Fox01-Forkhead Box Protein O1
GAPDH-Glyceraldehyde 3-Phosphate Dehydrogenase
Grb10-Growth Factor Receptor-Bound Protein 10 (AKA insulin receptor-binding protein)
GSK3-Glycogen Synthase Kinase 3
HK1- Hexokinase 1
HSP90- Heat Shock Protein 90
HNF4α- Hepatocyte Nuclear Factor 4 Alpha
IDH1-Isocitrate dehydrogenase 1 (AKA NADP+)
IRSI- Insulin Receptor Substrate-1
LBK1- Liver Kinase B1 (AKA Serine/threonine kinase 11)
LC3- Microtubule-associated Protein 1A/1B-Light Chain
LC-MS- Liquid Chromatography Mass Spectrometry
Mdx- Murine model of Duchenne's Muscular Dystrophy
mTOR- Mammalian target of rapamycin
mRNA- Messenger RNA
MyH2- Myosin Heavy Chain form 2
MyH4- Myosin Heavy Chain form 4
MyH7- Myosin Heavy Chain form 7
NRF1-Nuclear respiratory factor 1
NRF2- Nuclear respiratory factor 2
OCR- Oxygen Consumption Rate
OXPHOS- Oxidative phosphorylation
P62-Nucleoporin P62
PGC1α-Peroxisome Proliferator-Activated Receptor Gamma Coactivator 1-Alpha
PPARγ- Peroxisome Proliferator-Activated Receptor Gamma

Raptor- Regulatory-Associated Protein of mTOR
Rheb- Ras Homolog Enriched in Brain
RT-PCR – Real Time Polymerase Chain Reaction
SDH- Succinate Dehydrogenase
SEM- Standard Error of the Mean
TCA- Tricarboxylic Acid cycle
Tnni1- TroponinI 1
Tnnc1-TroponinC 1
Tnnt1- TroponinT 1
TSC2- Tuberous Sclerosis 2 (aka Tuberin)
UtrA- Utrophin A
WGA-Wheat Germ Agglutinin
YY1- Ying-Yang 1

Acknowledgements

This study was supported by NIH grants K26RR024462, P30CA015704, R56AI092093, P30-DK035816 and 1R25OD010450-01A1. I thank Michelle Loprieno for assistance with the fluorescent microscopy, FHCRC Electron microscopy core for help with EM images, Brian Johnson from the Histology and Imaging Core for assistance with immunohistochemistry.

I would like to thank Dr. Glen Banks for his expertise and assistance with regards to the many experiments involving muscle physiology and muscular dystrophy.

Thanks also to Dr. David Hockenbery and Dr. Daciana Margineantu for their help with the Seahorse assay as well as Dr. Daniel Raftery and Dr. Haiwei Gu for their assistance with mass spectrometry measurements.

Finally thanks to the wonderful research team in the Iritani lab:
Dr. Dinesh Hirenallur-S, Dr. Terri Iwata, Dr. Julita Ramirez, Mark Tsang, Michelle-Ann Torres and Jacky Chan

As well as to my mentor Dr. Brian Iritani, without whom none of this research would have been possible.

Dedication

This work is dedicated to my wonderful wife who has supported me through these years of research and to my father from whom I inherited my love for medicine.

Introduction

Mammalian skeletal muscle is composed of a mosaic of muscle fiber types, which have varying capacities for strength and endurance dictated in part by differences in cytoskeletal morphology, mitochondrial density, and metabolic strategy. In particular, there are 4 recognized skeletal muscle fiber types (Type I, Type IIa, Type IIb, and Type IIx) which are defined based on structural and functional differences in the representation of myosin heavy chain (MyH) proteins, mitochondria and capillary density, power produced, fatigue resistance, and metabolic strategies (i.e. oxidative phosphorylation versus glycolysis). Type I "slow twitch" fibers are deep red in color due to high concentrations of Myoglobin and high densities of blood capillaries, which support sustained aerobic activity. Type I fibers are also rich in mitochondria, highly oxidative, and have increased contraction endurance with lesser strength potential. In contrast, Type IIa/b "fast twitch" fibers are pale in color due to low concentrations of Myoglobin, contain comparatively lower levels of mitochondria, and rely more heavily on anaerobic glycolysis for energy production. These characteristics allow type II fibers to have considerable strength and contraction speed, but only for short anaerobic bursts of activity before the muscles readily fatigue. Similar to Type IIa fibers, Type IIb/x fibers retain moderate strength capacity relative to fast twitch muscle fibers, but also have improved resistance to fatigue due to intermediate mitochondria levels and oxidative potential. Because slow twitch fibers predominantly utilize fatty acid oxidation relative to glucose (compared to fast-twitch fibers, which utilize glucose), increasing representation of type I fibers provides increased protection against obesity and related metabolic disorders [1-4]. Importantly, skeletal muscle fibers retain plasticity throughout adult life and can be interconverted as a result of exercise and a multitude of metabolic cues [5-7]. Hence, identifying molecules and signaling pathways that regulate fiber type conversion can have profound impacts on exercise physiology and susceptibility to metabolic diseases including obesity, diabetes, and muscular dystrophies, which are characterized by defective mitochondria.

Over the last decade, studies utilizing transgenic and knockout mice, as well as chemical agonists and antagonists, have resulted in the identification of several signaling molecules and transcription factors which regulate skeletal muscle fiber type differentiation. In particular, the master metabolic sensor AMP kinase (AMPK) has emerged as a key regulator of mitochondrial biogenesis, type I fiber type specification, and endurance adaptations during chronic exercise [8, 9]. AMPK is activated in response to metabolic cues such as low energy (high AMP/low ATP), changes in intracellular Ca^{2+}, and exercise (see [10] for review). Upon activation, AMPK stimulates mitochondrial biogenesis, ATP production, and autophagy (self-digestion to generate nutrients), while concurrently inhibiting ATP consumption mediated by mammalian target of rapamcin (mTOR), a major regulator of cell growth and protein synthesis. Inhibition of AMPK activity in mice results in reduced running capacity and impaired mitochondrial biogenesis [11, 12], whereas increased AMPK activation stimulates mitochondrial expansion in glycolytic skeletal muscle and increased resistance to fatigue [13, 14]. Importantly, recent developments suggest that many of the major benefits of endurance exercise on overall metabolic health are mediated in part by activation of AMPK, which stimulates expression of genes involved in slow twitch contractile apparatus, mitochondrial respiration, and fatty acid oxidation [8, 12, 14].

Over the past decade, there has been significant interest in understanding the pathways and molecules that synergize with or act downstream of AMPK to stimulate mitochondrial biogenesis and type I fiber type differentiation. This has resulted in the identification of several pathways and molecules including calcium signaling ((calmondulin kinase (CaMK) and the phosphatase calcineurin) [15, 16] [17, 18], and the nuclear regulator peroxisome proliferator-activated receptor-γ coactivator-1α (PGC1α). In particular, AMPK and Ca^{2+} signaling synergize to regulate expression and stability of PGC1α and PGC1β, which further activate entire genetic programs involved in mitochondrial biogenesis, oxidative metabolism, and slow twitch fiber specification. Constitutive deletion of PGC1α expression results in a significant decrease in

expression of genes associated with mitochondrial protein translation and function [19, 20]. Skeletal muscle specific deletion of PGC1α induces a pronounced muscle fiber type shift from Type I and Type IIa muscle fibers towards more glycolytic Type IIb/x fibers resulting in a loss of endurance and an increased susceptibility to post-exercise muscle fiber injury[21]. Conversely, skeletal muscle-specific PGC1α over-expression produces a dramatic shift towards highly oxidative Type I fibers exhibiting increased endurance capacity in muscles which are predominantly fast twitch [3, 21] AMPK phosphorylates [22] and up-regulates expression of PGC1α indicating that AMPK may modulate fiber type specification, in part through PGC1α. However, the molecules that link AMPK to PGC1α signaling remain elusive.

Through the use of a random ENU mutagenesis strategy in mice to identify novel immune regulatory genes[23], we previously identified a mouse pedigree which lacks expression of Folliculin Interacting Protein-1 (Fnip1) due to a 32-bp deletion in the *Fnip1* gene[24]. *Fnip1*$^{-/-}$ mice were identified by an absence of circulating B lymphocytes, which was attributed to a block in B cell development and survival at the pre-B cell stage[24]. Although the functions of Fnip1 are poorly understood, Fnip1 protein interacts with Folliculin, Fnip2 (a related Fnip family member), and all three subunits (α, β, γ) of AMPK [25][26, 27]. Mutations in the *Bhd* gene encoding Folliculin results in Birt-Hogg-Dube (BHD) Syndrome, a rare human condition characterized by hamartoma formation, pulmonary cysts, and development of renal tumors[28]. In the current study, we found that loss of Fnip1 results in a dramatic shift of skeletal muscle fiber type towards Type I slow twitch fibers, due in part to increased activation of AMPK and PGC1α. These results identify a novel pathway involving Fnip1 in the differentiation of skeletal muscle fiber types, and suggest that Fnip1 may provide a novel link between AMPK and PGC1α.

Materials and Methods

Transgenic animals

Fnip1$^{-/-}$ mice were developed as previously described[24]. *PGC1α*[29] and *Dmd*^{Mdx4CV}[30] mice were obtained from Jackson Laboratories and the Chamberlain laboratory respectively. Mice were housed under specific-pathogen-free conditions. All experiments were reviewed and approved by the Institutional Care and Use Committee of the University of Washington.

Special diets

Rapamycin diet was milled at TestDiet (Richmond, IN) and impregnated with rapamycin (14ppm) in the lab of Dr. Randy Strong at the University of Texas Health Center, Barshop Institute (San Antonio, TX). All mice were approximately age and sex-matched. Breeding pairs were started on Rapamycin diet. Mice in the rapamycin treatment group were continued on rapamycin chow after weaning and continued for a total of 6 weeks. After completion, all animals were euthanized via CO_2 asphyxiation and the gastrocnemius muscles were harvested.

Immunoblot analysis

Tissue for immunoblotting and RNA analyses were flash frozen and stored at -80 degrees Celsius until lysis. Frozen gastrocnemius muscles were homogenized in a hypotonic lysis buffer (50mM HEPES, 150mM NaCl, 1% Trition 100x, 150mM $MgCl_2$, 10% glycerol, 1mM EGTA, 1mM EDTA) with Halt Protease and Phosphatase Inhibitor™ (Thermo Scientific Rockford, IL). Protein concentrations were determined via the Micro BCA™ Protein Assay Kit (Thermo Scientific, Rockford, IL). An equal amount of protein lysate from each sample (30-60ug) was loaded in each lane and protein components were separated via sodium dodecyl sulfate-polyacrylamide gel electrophoresis (SDS-page) through 6-12% gels Protein bands were

transferred to a Protran BA 83 Nitrocellulose Membrane (Whatman Inc. Florham Park, NJ). After blocking in 3% milk, blots were incubated overnight in primary antibodies against phospho-S6R, phospho-AMPK ser172, total AMPK, mTor, phospho-Raptor, phospho-4EBPI, LC3B (Cell Signaling Technology. Danvers, MA), PGC1-alpha (Millipore, Temecula California) and Myoglobin (Santa Cruz Biotechnology) followed by incubation with horseradish peroxidase-conjugated (HRP) secondary antibody. The MyH7 antibody (A4.840) developed in the lab of Helen Blau and was obtained from the Developmental Studies Hybridoma Bank developed under the auspices of the NICHD and maintained by The University of Iowa, Department of Biology, Iowa City, IA. 52242. Utrophin A antibody was produced in the lab of Dr. Stanley Froehner at the UW. Antibody–bound proteins were visualized through *SuperSignal West Pico HRP Chemiluminescent Substrate* (Thermo Scientific. Waltham, MA) activated exposure on GeneMate Blue Basic Autorad Double Emulsion Radiograph Film (Bioexpress Kaysville, UT).

Realtime-PCR

Frozen tissue was converted to RNA with the use of RNAqueous 4-PCR Kit (Ambion Inc. Austin, TX). Synthesized cDNA was yielded from RNA lysate via Invitrogen SuperScript II Reverse Transcriptase (Life Technologies Grand Island, NY). All oligonucleotide primers for RT-PCR were produced by Integrated DNA Technologies (Coralville, IA). Full primer sequences are listed in [24] and Supplemental Materials. PCR reactions were performed using the SYBR green system with annealing temperatures at 57-60^{o}C. Quantitative values of each sample were calculated by paired comparison of $\Delta\Delta C_T$ values (n=3-6/group).

Immunohistochemistry and Metachromatic ATPase Staining

The gastrocnemius muscle was collected from *Fnip1*$^{-/-}$, *Fnip1*$^{-/-}$ and *Rag1*$^{-/-}$ mice (Rag null tissues were collected as a negative control for cross reaction of anti-mouse secondary antibodies

when using mouse primary antibodies). Collected tissues were flash frozen in OCT before sectioning. All special staining was performed at the University of Washington's Histology and Imaging Core (HIC). MyH7 antibody was obtained from Sigma Aldrich (St. Louis, MO).

Muscle Morphometry

Samples of fresh gastrocnemius muscles taken from Wt, *Fnip1*$^{-/-}$, *Mdx*$^{4CV-/-}$ and *Fnip1*$^{-/-}$*Mdx*$^{4CV-/-}$ double knockout mice were snap frozen in OCT (n=3/genotype). 5 micron cross sections were mounted on slides and fixed with paraformaldehyde. Slides were stained with a fluorescent antibody against Wheat Germ Agglutinin (WGA) to highlight plasma membrane specific glycoproteins and counterstained with 4',6-Diamidino-2-Phenylindole, Dihydrochloride (DAPI). Resulting images were analyzed at 100x magnification. In order to measure myofibril cross sectional area groups of 10 adjacent myofibers (total of 100 fibers) were chosen at random (n=3/genotype) and their diameters traced. Resulting traces were analyzed in an imaging analysis program (ImageJ: http://imagej.nih.gov/ij/) to provide relative surface area. In these same images, DAPI positive staining nuclei were manually counted in 10 separate fields at 200x magnification. Readers were blinded and fields randomly chosen. Nuclei were categorized as centrally or peripherally positioned for comparison. Additionally, quadriceps muscles from each of these animals were fixed in 10% buffered formalin and resulting slides were stained with H&E.

Seahorse metabolic analyses

Gastrocnemius muscles were collected from *Fnip1*$^{-/-}$ and *Fnip1*$^{+/-}$ (wildtype) mice that were age and sex-matched. Fresh tissue was rinsed in phosphate buffered saline and placed in a dissociation media composed of Dulbecco's Modified Eagle Medium (DMEM), gentamycin, 2% fetal bovine serum and Collagenase A and left to incubate at 37 degrees Celsius at 5% carbon

dioxide for 1.5-2 hours. Muscle samples were then removed from dissociation media and gently triturated in DMEM until single muscle fibers were detached and suspended in solution. Isolated fibers of each genotype were combined and plated in replicate. After visualization under a dissecting microscope, fibers were counted and plated equivalently with a target confluence of 80-90%. Fibers were cultured on matrigel media in an *XF96 microplate (Seahorse Biosciences)* and incubated at 37 degrees Celsius for 6-12 hours prior to analysis. Mitochondrial function was analyzed in accordance with the *XF Cell Mito Stress Test Kit (Seahorse Biosciences)* and basal respiratory and glycolytic rates will be determined. Following basal measurements, multiple assays reagents were added including: carbonyl cyanide 4-(trifluoromethoxy) phenylhydrazone (FCCP; Sigma C2920) and Antimycin.

Muscle fatigue assay

8 week-old male *Fnip1*$^{-/-}$ and WT control mice were anesthetized intraperitoneally with Avertin (17ul/kg body weight, 2.5% solution) with supplemental doses administered as required to maintain necessary anesthesia. A small incision was made to expose the Achilles tendon. The intact tendon was attached to the lever arm of the servometer (Cambridge Technology Model 305) which measures applied force during initiated contraction. The hindlimb was stabilized and needle electrodes were inserted on either side of the tibial nerve. The stimulation voltage and muscle length are adjusted for maximum isomeric twitch force. The signal output of the force transducer was displayed on a storage oscilloscope (Tektronix Model 5111) coupled to a microcomputer used for data acquisition and storage. The muscle is then stimulated every 2 seconds for a total of 4 minutes and then allowed to recover briefly. At three and five minutes post contraction single stimulations were performed and force measured to assess recovery capacity. Specific force was calculated as peak titanic force x muscle length x pennation (0.45 for gastrocnemius) x density (1.04)/muscle mass.

Transmission electron microscopy

Fresh samples of the gastrocnemius muscles harvested from 8 week-old male *Fnip1* null and WT control mice were chopped into 1mm cubes and preserved in Karnovsky's Gluteraldehyde fixative. Samples were dehydrated, sectioned into 70-100nm sections at the Electron Microscopy Core Facility of the Fred Hutchinson Cancer Research Center (Seattle, WA). Tissue slices were epoxy embedded and visualized with the use of a JEOL 1400 transmission electron microscope (JEOL Ltd., Tokyo, JAPAN).

Serum creatine kinase assay

Creatine Kinase (CK) was measured from serum collected from age-matched mice via retroorbital bleeds. Measurement was performed using the Creatinine Kinase- SL Reagent Kit (Seikisui Diagnostics P.E.I. Inc. PE Canada). Colorimetric results were read at 340nm after two minutes of incubation at 37 degrees C and then each minute for the following two minutes. The average change in absorbance per minute was multiplied by a factor of 6592 to yield international units/L (IU/L).

Evans blue dye assay

A 1% solution of Evan's Blue Dye was injected intraperitoneally into Wt, *Fnip1*$^{-/-}$, *Mdx*$^{4CV-/-}$ and *Fnip1*$^{-/-}$*Mdx*$^{4CV-/-}$ double knockout mice (n=3/group) at a volume dose of 1% of body weight. Approximately 20 hours following injection mice were sacrificed and the gastrocnemius muscles were isolated and snap frozen in OCT media. Leakage of Evans blue dye was analyzed by fluorescence microscopy.

Results

Loss of Fnip1 increases the representation of type I skeletal muscle fibers

Upon gross observation, skeletal muscle from *Fnip1*$^{-/-}$ mice appeared dark red in coloration with reduced overall mass when compared to skeletal muscle from wildtype (WT) littermate control mice (Figures 1, 11A). Because slow-twitch fibers appear deeper red in coloration relative to fast-twitch fibers, we investigated whether loss of Fnip1 alters the representative composition of skeletal muscle fiber types. We stained histologic sections of gastrocnemius muscles from *Fnip1*$^{-/-}$ and wildtype mice for enzymes and proteins which are differentially expressed in Type I fibers relative to Type II fibers, including Succinate Dehydrogenase ([SDH], a critical mitochondrial enzyme involved in oxidative respiration), metachromatic ATPase ([pH 4.3] which allows for differential myofibrillar stain uptake based on oxidative ATPase activity), and Myosin Heavy Chain 7 ([MYH7], an isoform of MHC found in Type I Fibers). As shown in Figure 2, normal gastrocnemius muscle contains a mixture of SDH-positive type I and SDH-negative type II fibers. However, *Fnip1*$^{-/-}$ gastrocnemius muscle contains almost exclusively SDH positive type I fibers. *Fnip1*$^{-/-}$ muscle also contains an excess of strongly staining ATPase positive fibers relative to muscle from wildtype mice. This alteration correlates closely with an increase in muscle fibers expressing slow twitch specific MyH7. Morphometric analyses with anti-wheat germ agglutinin (WGA) revealed that *Fnip1* null skeletal muscle fibers are smaller in diameter relative to Wt skeletal muscle fibers (Figure 3), which is consistent with increased type I myofibers.

To further define the apparent shift in skeletal muscle fiber types following loss of Fnip1, we performed real-time PCR (RT-PCR) and immunoblotting for RNA and proteins characteristic of type I versus type II skeletal muscle fibers. RT-PCR revealed an approximately 3-fold increase in *Myoglobin* mRNA expression in *Fnip1*$^{-/-}$ skeletal muscle when compared to controls,

as well as pronounced increases in mRNA expression of cytoskeletal markers of slow twitch muscle including *Troponin I* slow (*Tnni1*, (~151 fold increase)), *Tnnc1* (~160 fold increase), *Tnnt1* (~400-fold increase), and *MyH7* (>800 fold increase) (Figure 4A), with corresponding decreases in the mRNA expression of MyH2 and MyH4, which are markers of Type II fibers. Immunoblot analyses confirmed significant increases in Myoglobin, MyH7, and Cytochrome C protein in *Fnip1* null mice when compared to wildtype controls (Figure 4B). These results collectively suggest that loss of Fnip1 results in a significant shift in the representation of skeletal muscle fibers from Type II to Type I fibers.

Fnip1 is normally expressed type II skeletal muscle fibers

To further define the role of Fnip1 in fiber type specification, we assessed the normal expression of Fnip1 protein in muscles with type II characteristics (extensor digitalis longus (EDL), gastrocnemius) versus type I characteristics (Soleus). We found that in wild-type skeletal muscles, Fnip1 protein is normally highly expressed in muscles known to be rich in type II fibers (EDL, gastrocnemius), but is low or absent in soleus muscles, which are rich in type I fibers (Figure 5). These results are consistent with the notion that Fnip1 has a significant role in fiber type specification.

Fnip1 null skeletal muscle contains increased numbers of highly functional mitochondria

To characterize the consequences of Fnip1 loss on the metabolic capacity of muscle fibers, we assessed the expression of key mitochondrial genes and measured the metabolic capacity of isolated myofibrils from *Fnip1*$^{-/-}$ and WT gastrocnemius muscle. RT-PCR analysis indicated that relative to WT skeletal muscle, disruption of Fnip1 resulted in increased expression of

mitochondrial genes which are more highly expressed in Type I fibers including genes involved in mitochondrial metabolism such as cytochrome B (*Cytb*; ~40-fold increase), ATP synthase lipid binding protein (*Atp5γ1*;~80-fold increase), uncoupling protein 3 (*Ucp3*;~18 fold increase), Isocitrate dehydrogenase 1 (*Idh1*; ~8-fold increase), and Hexokinase 1 (*Hk1*; ~22-fold increase) (Figure 6A). Disruption of *Fnip1* also results in dramatic increases in subsarcolemmal mitochondrial number, as determined by transmission electron microscopy (Fig. 8).

To assess the functional consequences of the excess mitochondria mass in *Fnip1*$^{-/-}$ skeletal muscle, we isolated adult myofibers from *Fnip1*$^{-/-}$ and WT mice and assessed basal metabolism using the Seahorse XF analyzer, which measures oxygen consumption rate (OCR; a measure of oxidative phosphorylation) and extracellular acidification rate (ECAR; a measure of glycolysis) on live cultured cells. Results of seahorse analyses showed that *Fnip1*$^{-/-}$ skeletal muscle myofibrils exhibit significantly increased basal (Figure 6B) and stimulated (not shown) oxygen consumption rates relative to wild-type myofibrils, whereas aerobic glycolysis was relatively unaffected. These results collectively suggest that disruption of *Fnip1* results in a pronounced expansion of functional mitochondria, which is consistent with a shift towards a predominance of highly oxidative skeletal muscle fibers with type I characteristics.

In order to better define this observed metabolic shift, we took an unbiased global metabolomic approach using liquid chromatography mass spectrometry (LC-MS) to measure alterations in levels of 168 metabolites associated with major metabolic pathways. We found that *Fnip1*$^{-/-}$ gastrocnemius muscle contains increased metabolites associated with amino acid signaling and progression of the TCA cycle, consistent with increased mTOR signaling (further discussed below) and increased oxidative metabolism (Figure 7). Collectively, our results are consistent with a normal role for Fnip1 in the generation and/or maintenance of Type II fibers, and a shift from predominantly type II fibers to Type I fibers following disruption of *Fnip1*.

Increased activation of AMPK and PGC1α in Fnip1 null skeletal muscle

Because Fnip1 physically interacts with AMPK, we compared RNA and protein levels of components of the AMPK signaling pathway in gastrocnemius muscle from *Fnip1* null and wild-type control mice. Levels of phosphorylated AMPK at threonine 172 were increased in *Fnip1*$^{-/-}$ skeletal muscle relative to WT skeletal muscle, which is indicative of activated AMPK (Figure 9A). Additionally, we found increased levels of phosphorylated-Acetyl CoA carboxylase 1 (ACC1), a protein involved in fatty acid synthesis that is switched off by AMPK phosphorylation. Importantly, expression of the transcriptional co-activator PGC1α, a principal regulator of mitochondrial biogenesis, was significantly elevated at both the protein (Fig. 9A) and RNA (Fig. 9B) level in skeletal muscle from *Fnip1*$^{-/-}$ relative to WT mice. Expression of PGC1α is known to be positively regulated by AMPK [12, 22]. Expression of *Pparγ* (a target of PGC1α) was also increased in *Fnip1*$^{-/-}$ mice. These results collectively suggest that disruption of *Fnip1* results in increased basal activation of AMPK and PGC1α in skeletal muscle tissue.

Increased mTORC1 and decreased autophagy in Fnip1 null skeletal muscle

Mammalian target of rapamycin mTOR consists of the rapamycin-sensitive mTORC1 complex (mTOR, Raptor, Pras-40, Deptor, mLST8) and the rapamycin-insensitive mTORC2 complex (Rictor, mSin1, Protor, Deptor, and mLST8). mTORC1 promotes cell growth by inducing anabolic processes and cell cycle progression in response to amino acids and growth factors. In contrast, mTORC2 regulates cell survival and cytoskeletal organization in response to growth factor signals. In the presence of low oxygen and energy deficit, activated AMPK inhibits energy consuming cellular growth driven by the mTORC1 pathway in part by phosphorylation and activation of the mTORC1 inhibitor TSC2, and by phosphorylation and inhibition of the mTORC1 activator Raptor. To determine if mTORC1 is regulated by Fnip1, we compared RNA and protein levels of components of the mTORC1 pathway in gastrocnemius muscle from *Fnip1*$^{-}$

$^{-/-}$ mice and wild-type control mice. Immunoblot analysis revealed increased phosphorylated ribosomal S6 protein (S6R) and increased phosphorylated EIF4E-binding protein (P-4EBP) in *Fnip1*$^{-/-}$ muscle relative to WT muscle (Fig. 10A). P-S6R and P-4EBP are downstream products of mTORC1 activation and are commonly used as markers of mTORC1 activity. Active mTORC1 is known to negatively feedback to inhibit mTORC1 activation, in part by phosphorylating IRS1 and the receptor tyrosine kinase inhibitor growth factor receptor-bond protein 10 (Grb10), and by reducing expression of growth factor receptors[31]. Indeed, we find a dramatic reduction of biphosphorylated Glycogen Synthase Kinase-3 (GSK-3) which is phosphorylated at both alpha and beta subunits (Ser 21, Ser9 respectively) by Protein Kinase B (AKT), a downstream effector of PI3 kinase (Fig. 10A). Inhibition of GSK activation is likely a consequence of mTORC1 hyperactivation and subsequent negative feedback inhibition through inhibition of PI3-kinase and subsequently AKT.

mTORC1 also promotes cell growth by negatively regulating autophagy, an energy producing process in which cytoplasm and organelles are enveloped into structures known as autophagosomes and subsequently degraded into components which can be of use to the cell. To determine if Fnip1 null mice showed derangement in normal autophagic balance we performed western blots on skeletal muscle protein isolates, probing for autophagic protein markers such as microtubule associated protein light chain LC3B and ubiquitin binding protein P62, which are widely utilized as markers of autophagy. We found increased ratio of LC3I to LC3II and increase P62 in *Fnip1*$^{-/-}$ versus Wt skeletal muscle, which is indicative of impaired autophagy and hyperactivation of mTOR (Fig 10A). We next examined whether hyperactive mTOR and impaired autophagy might be responsible for the shift in skeletal muscle fiber type following disruption of *Fnip1*. We treated *Fnip1* null mice with the mTORC1 inhibitor rapamycin beginning at conception (i.e. breeding pairs were treated with rapamycin diet) through weaning until 6 weeks of age, when skeletal muscle was harvested and analyzed by immunoblot. We

found that long-term rapamycin failed to rescue normal fiber type representation despite inhibition of mTORC1 activity to below basal Wt levels (Figure 10B). Rapamycin failed to reduce levels of the slow twitch marker MyH7, Myoglobin, and PGC1α, in *Fnip1*$^{-/-}$ mice relative to WT mice. However, rapamycin nearly completely restored normal autophagy based on increased LC3BI:LC3BII ratio, which is consistent with the known ability of mTORC1 to inhibit autophagy. These results collectively support a role of Fnip1 in skeletal muscle fiber type representation relatively independent of mTORC1 and impaired autophagy.

Fnip1 null skeletal muscle generates less force and is more resistant to fatigue

To investigate the functional significance of the shift in fiber type following disruption of Fnip1, we performed an *in situ* muscle fatigue assay to evaluate contraction characteristics of gastrocnemius muscle from anesthetized *Fnip1*$^{-/-}$ and WT mice. This assay specifically tests skeletal muscle endurance by examining the functions of single isolated muscle bellies at normal body temperature and under optimal perfusion conditions. This eliminates decision-based variables and/or endurance disparity due to systemic illness. We found that intact *Fnip1*$^{-/-}$ gastrocnemius muscles were smaller and weighed significantly less than that of the wild-type controls (Fig. 11A), consistent with a switch to a preponderance of type I fibers. Additionally *Fnip1*$^{-/-}$ gastrocnemius muscles exhibited considerably reduced baseline force capacity compared to Wt mice generating approximately one half the initial peak force as was seen in Wt mice (Figs. 11B and C). Following repeated stimulation, the forces of contraction dropped progressively in both wild-type and *Fnip1*$^{-/-}$ null mice. Within 60 seconds of recurrent contraction, both strains of mice reached a trough force level which remained steady with minimal decay on continued stimulation. Interestingly, whereas *Fnip1*$^{-/-}$ mice plateaued at approximately 50 percent of peak force output, wild-type mice dropped much further reaching trough levels of approximately 30 percent of initial peak force (Figs. 12A and B). Furthermore,

following repeated contraction, *Fnip1* null mice recovered significantly quicker compared to Wt controls, returning to approximately 100 percent of baseline peak force within 3 minutes following contraction (Figure 12C), whereas control gastrocnemius muscles remained at approximately 85 percent of peak following the same recovery period. The increased endurance and resistance to fatigue following disruption of Fnip1 is consistent with a shift in fiber type ratio towards highly oxidative slow twitch fibers.

Loss of Fnip1 stimulates Type I Fiber type differentiation in a PGC1α dependent manner

PGC1α is a key driver of metabolic reprogramming, mitochondrial biogenesis, and type I fiber specification in skeletal muscle. Because disruption of Fnip1 results in increased expression of PGC1α (Figure 9A), we sought to determine if the muscle fiber shift observed in *Fnip1* null mice is due in part to the induction of PGC1α. We bred *Fnip1*$^{-/-}$ mice with *PGC1α* null mice[29] to generate *Fnip1*$^{-/-}$ *PGC1α*$^{-/-}$ double-null mice. Upon gross examination, disruption of *PGC1α* appeared to partially restore normal coloration of *Fnip1*$^{-/-}$ skeletal muscle (Figure 13A). Immunoblot analysis of total protein taken from the gastrocnemius muscle revealed a dramatic reduction in slow twitch myosin (MyH7), Cytochrome C, and total Myoglobin in *Fnip1*$^{-/-}$ *PGC1α*$^{-/-}$ mice when compared to *Fnip1*$^{-/-}$ mice (Figure 13B) suggesting a partial rescue of the oxidative phenotype. Additional blots showed a reduction in phosphorylated-Acetyl CoA carboxylase 1 (ACC1) levels in double knockout mice when compared to *Fnip1*$^{-/-}$, indicative of a reduction in AMPK hyper-activation characteristic of the *Fnip1*$^{-/-}$ skeletal muscle phenotype. These findings identify *PGC1a* as an essential mediator of the oxidative muscle fiber shift seen in *Fnip1* null mice.

Disruption of Fnip1 prevents muscular dystrophy in a murine model of Duchenne Muscular Dystrophy

Duchenne muscular dystrophy (DMD) is a fatal recessive X-linked hereditary disease characterized by progressive muscular dystrophy, which ultimately leads to paralysis and death from respiratory and/or cardiac failure[32]. DMD is caused by mutations in the *DMD* gene encoding dystrophin[33-35], a subsarcolemmal protein which functions as part of the dystrophin-associated glycoprotein complex (DGC). Disruption of the DGC complex in DMD leads to mitochondrial dysfunction, sarcolemmal ruptures, muscle fiber necrosis, and eventually irreversible muscle wasting. Since *Fnip1*$^{-/-}$ mice have increased numbers of functional mitochondria and increased fatigue resistance, we sought to determine if disruption of Fnip1 could ameliorate DMD disease. We bred *Fnip1*$^{-/-}$ mice to *Dmd*$^{mdx\text{-}4CV}$ mice[30] (herein mdx), which have a C- to T-transition in exon 53 that creates a non-sense codon resulting in the absence of Dystrophin protein [36]. To examine the effects of *Fnip1* loss on muscle morphology in mdx mice, we stained cross sections of Wt, *Fnip1*$^{-/-}$, mdx, and mdx*Fnip1*$^{-/-}$ gastrocnemius muscle with hematoxylin and eosin (Figs. 14, top and 15A, top), and anti-WGA combined with DAPI (Figs. 14, bottom and 15A, bottom) to better visualize muscle boundries and nuclei. As has been previously shown, we found that skeletal muscle fibers from mdx mice have increased numbers of centralized nuclei, which is a reflection of fiber regeneration following muscle injury. Concurrent disruption of *Fnip1* in mdx mice led to a ~50% reduction in the percentage of centrally located nuclei indicative of a decrease in muscle fiber injury. To more directly test the consequences of *Fnip1* loss on sarcolemmal rupture and muscle damage, we measured the extravasation of Evan's Blue Dye (EBD) in gastrocnemius muscle 20 hours after intravenous injection. EBD extravasation is a common measure of increased vascular and cellular permeability which occurs following muscle damage. We found a significant increase in Evans's blue extravasation in mdx muscle relative to Wt muscle (Figures 16A), as has been previously

shown. Disruption of Fnip1 in *Fnip1*$^{-/-}$mdx muscle reduced Evans blue extravasation to undetectable levels, as is seen in Wt mice. To further assess the potential benefits of *Fnip1* loss on inhibiting muscle damage in mdx mice, we measured the levels of serum creatine kinase (CK), which is a highly sensitive and widely utilized measure of muscle damage in mdx mice. As expected, mdx mice had a 17-fold mean increase in levels of CK relative to normal Wt mice (Figure 16B). Remarkably, disruption of *Fnip1* completely rescued serum CK levels in mdx mice to levels similar to that of wild type mice. Prevention of muscle damage in mdx*Fnip1*$^{-/-}$ mice is not due to up-regulation (compensation) of the dystrophin homolog utrophin, which is reduced in mdx*Fnip1*$^{-/-}$ mice relative to mdx mice (Figure 17). These results collectively indicate that inhibition of Fnip1 provides significant protection against muscle damage in a murine model of Duchenne muscular dystrophy in a utrophin independent manner.

Discussion

The benefits of endurance exercise on skeletal muscle function and resistance to obesity occur in part through the metabolic reprogramming of myofibers, which results in improved energy substrate utilization, contractile properties, and ultimately changes whole-body metabolism. In particular, endurance exercise increases the representation of Type I slow-twitch fibers which are rich in ATP-generating mitochondria and contain slow isoforms of contractile proteins that preferentially oxidize fatty acids and more fatigue resistant than Type II fast twitch fibers, which preferentially metabolize glucose and express fast isoforms of contractile proteins. Having a surplus of highly oxidative type I fibers results in considerable health benefits including increased protection against obesity and metabolic diseases including diabetes and cardiovascular disease [1-4]. In this study, we found that disruption of Fnip1 results in a dramatic shift in skeletal muscle fiber type from predominantly Type IIa glycolytic fibers to Type I oxidative fibers that are rich in mitochondria and preferentially utilize oxidative phosphorylation over glycolysis. These results identify Fnip1 as a new member of a signaling pathway involved in reprogramming skeletal muscle fiber specification, and that inhibition of Fnip1 has "exercise mimetic" properties, which has potential to profoundly impact overall metabolic health.

Relative to WT skeletal muscle, *Fnip1* null skeletal muscle is uniformly deep red in color (due in part to increased Myoglobin content), contains increased mitochondria (as determined by SDH staining, EM, and analysis of mitochondrial gene expression), and are greatly enriched for genes and proteins which characterize Type I fiber specification including MyH7, Cytochrome C, Tnni1, Tnnc1, Tnnt1. The increased mitochondria density in *Fnip1*$^{-/-}$ skeletal muscle results in higher oxygen consumption rates in vitro and improved resistance to muscle fatigue *in vivo* relative to WT skeletal muscle, suggesting that the mitochondria in *Fnip1*$^{-/-}$ mice are highly functional. Type II myofiber specific genes including MyH2 and MyH4 are proportionally

decreased in *Fnip1*$^{-/-}$ skeletal muscle relative to muscle taken from Wt controls. These findings indicate that Fnip1 is an important regulator of mitochondrial biogenesis and skeletal muscle fiber type specification.

Considering that Fnip1 physically interacts with all three subunits of AMPK, we sought to determine whether disruption of *Fnip1* results in altered AMPK signaling. We found that AMPK is hyperactivated in *Fnip1* null skeletal muscle based on increased phosphorylation of AMPK at Thr172, and increased phosphorylation of ACC1, an AMPK target involved in lipid metabolism. AMPK has previously been shown to be a major signaling molecule involved in specifying skeletal muscle fiber type differentiation and mitochondrial biogenesis[37] in response to endurance exercise and chronic energy deprivation. For example, gain-of-function mutations in AMPK γ3 subunit (R225Q) in mice increases mitochondrial biogenesis and oxidative potential in glycolytic skeletal muscle, and provides protection from dietary-induced insulin resistance due to increased lipid oxidation[14]. Similarly, exercise training and the AMPK agonist AICAR increased oxidative fibers and running endurance in adult mice[8] and increased glucose uptake[38]. Conversely, reduced AMPK activity in AMPKα2 null mice lead to decreased skeletal muscle mitochondrial function and increased insulin resistance[39, 40], and transgenic mice defective for AMPK activation have reduced voluntary exercise[38, 41]. AMPK β1β2 null mice also have drastically reduced exercise capacity, mitochondrial content, and contraction-induced glucose uptake[11]. With these findings in mind, our results suggest that loss of Fnip1 may stimulate skeletal muscle mitochondrial biogenesis and fiber type determination in part by directly or indirectly regulating activation of AMPK.

In response to high AMP/low ATP ratio, LKB phosphorylates and activates AMPK. Once activated, AMPK coordinates catabolic signaling pathways to increase energy production, while inhibiting anabolic processes and energy consumption mediated by mTOR. More specifically, AMPK inhibits mTOR by phosphorylating and activating the mTOR inhibitor

TSC2[42] and phosphorylating and inhibiting the mTOR activator Raptor[43]. To determine if loss of Fnip1 alters mTOR signaling, we measured the activation of mTOR in isolated skeletal muscle from *Fnip1*$^{-/-}$ and WT mice. We found that mTOR activity is significantly elevated following disruption of Fnip1, based on increased phosphoryation of S6R and 4E-BP, which are downstream targets of mTOR. Previous studies indicate that activated mTOR promotes a strong negative feedback loop by phosphorylating insulin receptor substrate-1 [(IRS-1) which promotes IRS-1 degradation][44], and by phosphorylating growth factor receptor-bound protein 10 (Grb10)[44], which reduces growth factor signaling downstream of RTKs. Indeed, we found a dramatic reduction in phosphorylation of GSKα at the AKT phosphorylation site, which is indicative of reduced PI3 kinase signaling, an upstream activator of mTOR. We also found significant impairment of autophagy (self –digestion of organelles to generate nutrients), based on increased LC3BI-LC3BII ratio and increased p62 sequestome, which are widely utilized as markers of autophagy[45]. This inhibition was partially restored by treatment with rapamycin, suggesting that inhibition of autophagy is mediated at least in part through mTOR, a potent inhibitor of autophagy [46]. These results collectively suggest that disruption of Fnip1 results in hyperactivation of mTOR in skeletal muscle cells, perhaps by preventing the abilities of AMPK to efficiently inhibit mTOR.

Previous studies have suggested that mTORC1 is also necessary for the maintenance of mitochondrial oxidative function in skeletal muscle cells, in part by coactivating the mitochondrial biogenesis factor PGC1α and the *YING-YANG1* protein (YY-1)[47]. To determine if excessive mTOR is required for this shift in skeletal muscle phenotype, we treated mice with the mTORC1 inhibitor rapamycin for up to 12 weeks beginning in utero. Despite a >75% reduction in phospho-S6R in *Fnip1*$^{-/-}$ skeletal muscle (to levels below wildtype), rapamycin failed to restore normal representation of Type II fibers. However rapamycin did rescue the autophagic block observed in *Fnip1*$^{-/-}$ skeletal muscle. These results suggest that the

shift in skeletal muscle fiber type following disruption of Fnip1 is not likely a direct consequence of mTOR hyperactivation.

To further define the role of Fnip1 in the regulation of mitochondrial biogenesis and fiber type determination, we assessed the expression of PGC1α, a master transcriptional co-activator known to regulate these processes. PGC1α, and the related PCG1β, have been shown to activate a program of mitochondrial biogenesis and oxidative phosphorylation, by increasing components of the electron transport chain, TCA cycle, and fatty acid oxidation[48]. PGC1α is preferentially expressed in type I fibers, and transgenic expression of PGC1α[3] (or the related PCG1β[4]) in skeletal muscle fibers dramatically increases mitochondrial content, cellular respiration, endurance capacity, and fatigue resistance. Transgenic PGC1α in particular is sufficient to drive the formation of slow-twitch type I and IIa muscle fibers in muscle such as the *gastrocnemius* and *plantaris* which are predominantly composed of fast twitch myofibers[3]. Conversely, skeletal muscle specific deletion of *PGC*1α results in a muscle fiber type shift from Type I and Type IIa muscle fibers towards more glycolytic Type IIb/x fibers resulting in a significant loss of endurance and an increased susceptibility to post exercise muscle fiber injury[49]. In our study, we found that disruption of *Fnip1* results in increased expression of *PGC1α* mRNA and total protein, which correlated with increased mRNA expression of PGC1α target genes. Skeletal muscle from *Fnip1*$^{-/-}$ mice and *PGC1α* transgenic mice[3] have strikingly similar deep red coloration, indicative of a switch to Myoglobin-rich slow twitch muscle. To determine whether increased PGC1α is responsible for the increased representation of slow-twitch muscle fibers in *Fnip1*$^{-/-}$ mice, we generated *PGC1α*$^{-/-}$*Fnip1*$^{-/-}$ mice. We found that loss of PGC1α dramatically reduced expression of the slow-twitch specific MHC protein MyH7, as well as Myoglobin and Cytochrome C in *PGC1α*$^{-/-}$*Fnip1*$^{-/-}$gastrocnemius muscle relative to *Fnip1*$^{-/-}$ gastrocnemius

muscle. These results demonstrate that disruption of Fnip1 results in increased PGC1α protein, which in turn contributes to increased mitochondrial biogenesis and muscle fiber type switch.

Fnip1 physically interacts with Folliculin, Fnip2, HSP90, and all three subunits of AMP kinase. In the presence of high AMP, AMPK stimulates mitochondria biogenesis and increases oxidative phosphorylation to produce ATP, in part by increasing expression of *PGC1α* mRNA and by phosphorylating PGC1α [22], resulting in increased protein stabilization. In the absence of Fnip1, we find increased activation of AMPK, increased PGC1α protein levels, and increased activation of mTORC1 in *Fnip1*$^{-/-}$ relative to WT skeletal muscle. Whereas mTOR has also been shown to promote mitochondrial biogenesis by enhancing YY1 interaction and co-activation with PGC1α, long-term inhibition of mTORC1 with rapamycin fails to restore normal representation of slow twitch fibers in *Fnip1*$^{-/-}$ mice. In contrast, disruption of PGC1α rescues fiber type representation. These results collectively suggest that Fnip1 modulates mitochondrial biogenesis and skeletal muscle differentiation in a PGC1α dependent, mTOR independent manner. The mechanism, of how Fnip1 acts to inhibit PGC1α is unclear. However, AMPK has been shown to phosphorylate both Fnip1 and Folliculin, and inhibition of Folliculin also induces mitochondrial biogenesis and skeletal muscle fiber type switch in a PGC1α dependent manner[50]. Hence, the complex of Fnip1 and Folliculin may function in a negative feedback loop to inhibit or "turn off" AMPK, PGC1α, and oxidative metabolism following AMPK activation.

Muscular dystrophy diseases are often typified by defective mitochondria[51], and slow oxidative fibers have been shown to be more resistant to dystrophic pathology than faster, glycolytic fibers[52]. In this study, we found that inhibition of Fnip1 dramatically improves severe dystrophic pathology in the mdx murine model of Duchenne muscular dystrophy[21]. Skeletal muscle-specific overexpression of PGC1α also protects against muscle dystrophy,

suggesting that inhibition of Fnip1 may act in part through induction of PGC1α [53]. Given the role of Fnip1 in skeletal muscle fiber type differentiation, mitochondrial biogenesis and resistance to fatigue, these results suggest that pharmacological inhibition of Fnip1 may provide innovative strategy to improve muscle function on patients with muscular dystrophy diseases, and/or improve the responses of patients with obesity associated disease. In addition, whereas genetic disruption of either Folliculin or PGC1α is either embryonic or early post-natal lethal in mice, constitutive loss of Fnip1 is well tolerated suggesting that pharmacologic inhibition of Fnip1 may have low toxicity.

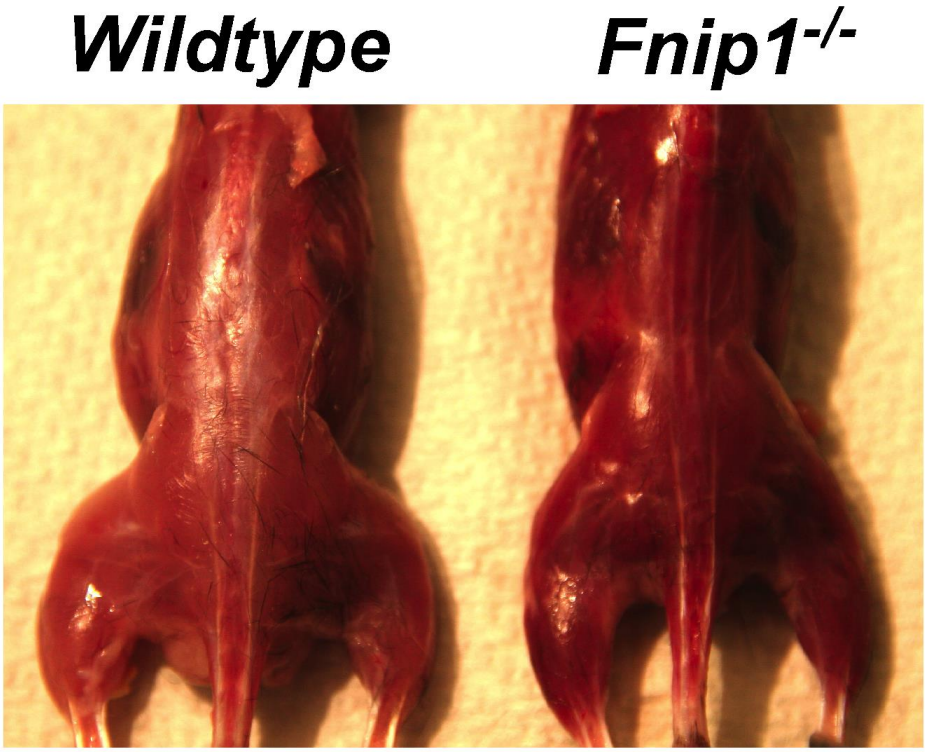

Figure 1. *Fnip1*$^{-/-}$ skeletal muscles are less prominent when compared to WT controls and display a characteristic deep reddish coloration.

Representative photographs showing wild-type and *Fnip1*$^{-/-}$ skeletal muscle shortly after euthanasia.

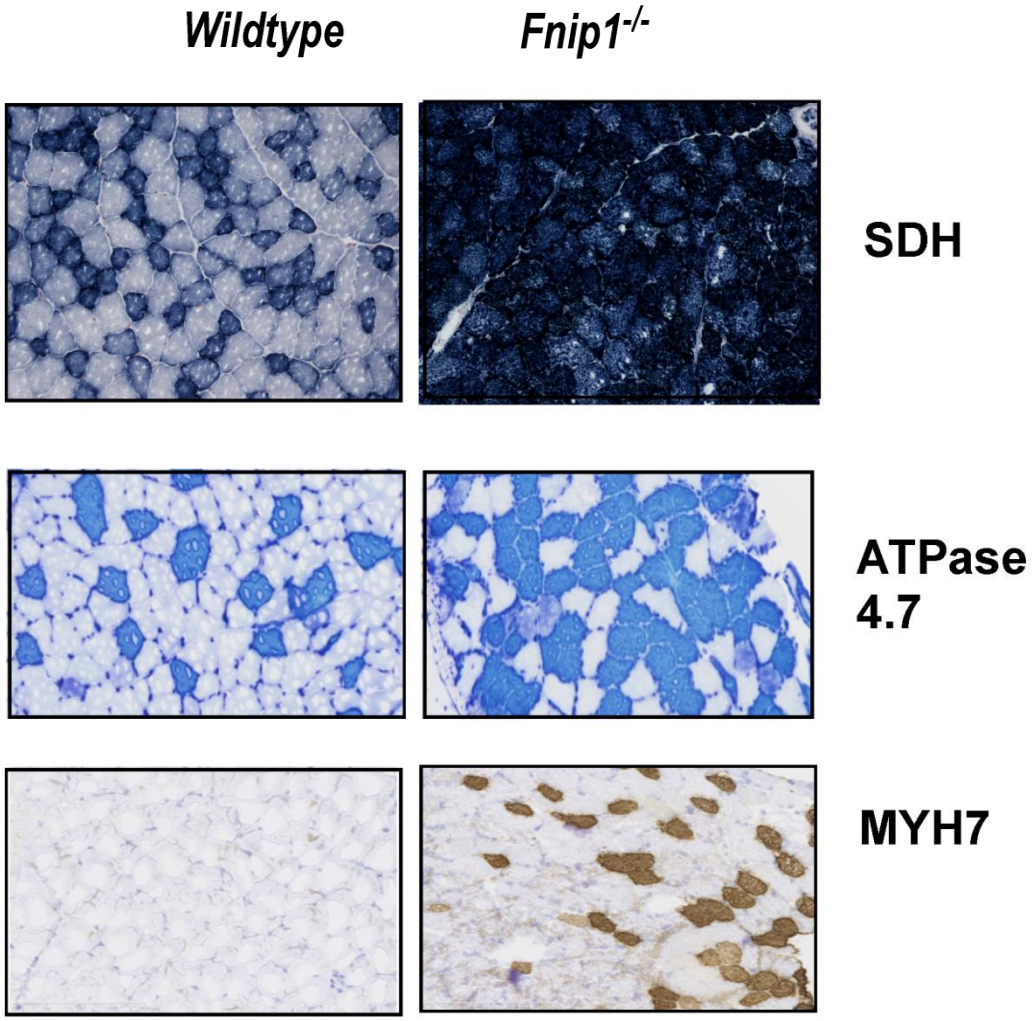

Figure 2. *Fnip1*$^{-/-}$ skeletal muscle contains a higher concentration of highly oxidative, slow twitch fibers.

Immunohistochemical staining of mitochondrial and slow twitch myofibril markers was performed on cross sections of the gastrocnemius muscle taken from 8-week old male *Fnip1*$^{-/-}$ mice and wild-type littermate controls. Shown are representative Succinate Dehydrogenase (SDH); ATPase (pH 4.7); and Myosin Heavy Chain 7 (MyH7) stained sections from N=3-5 mice per group.

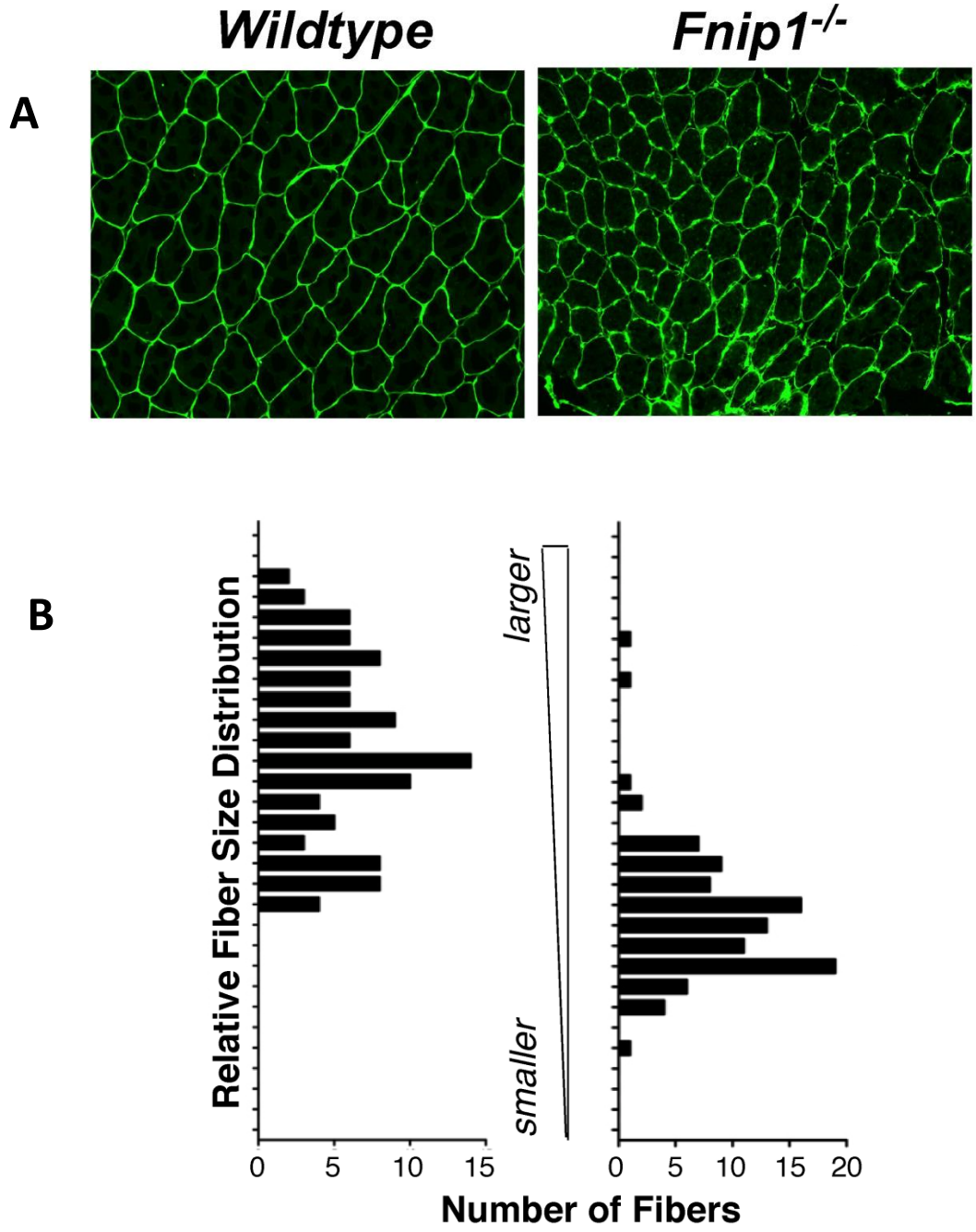

Figure 3. *Fnip1*$^{-/-}$ myofibrils are significantly smaller than those of WT controls.

(A) Representative wheat germ agglutinin (WGA) stained cross sections of WT and *Fnip1* null gastrocnemius muscles. Images were collected by fluorescence microscopy. **(B)** Bar graphs depict relative fiber size distribution of a total of 100 individual fibers (groups of 10 fibers chosen at random and cross sectional surface area measured) per genotype (n= 3 mice/group).

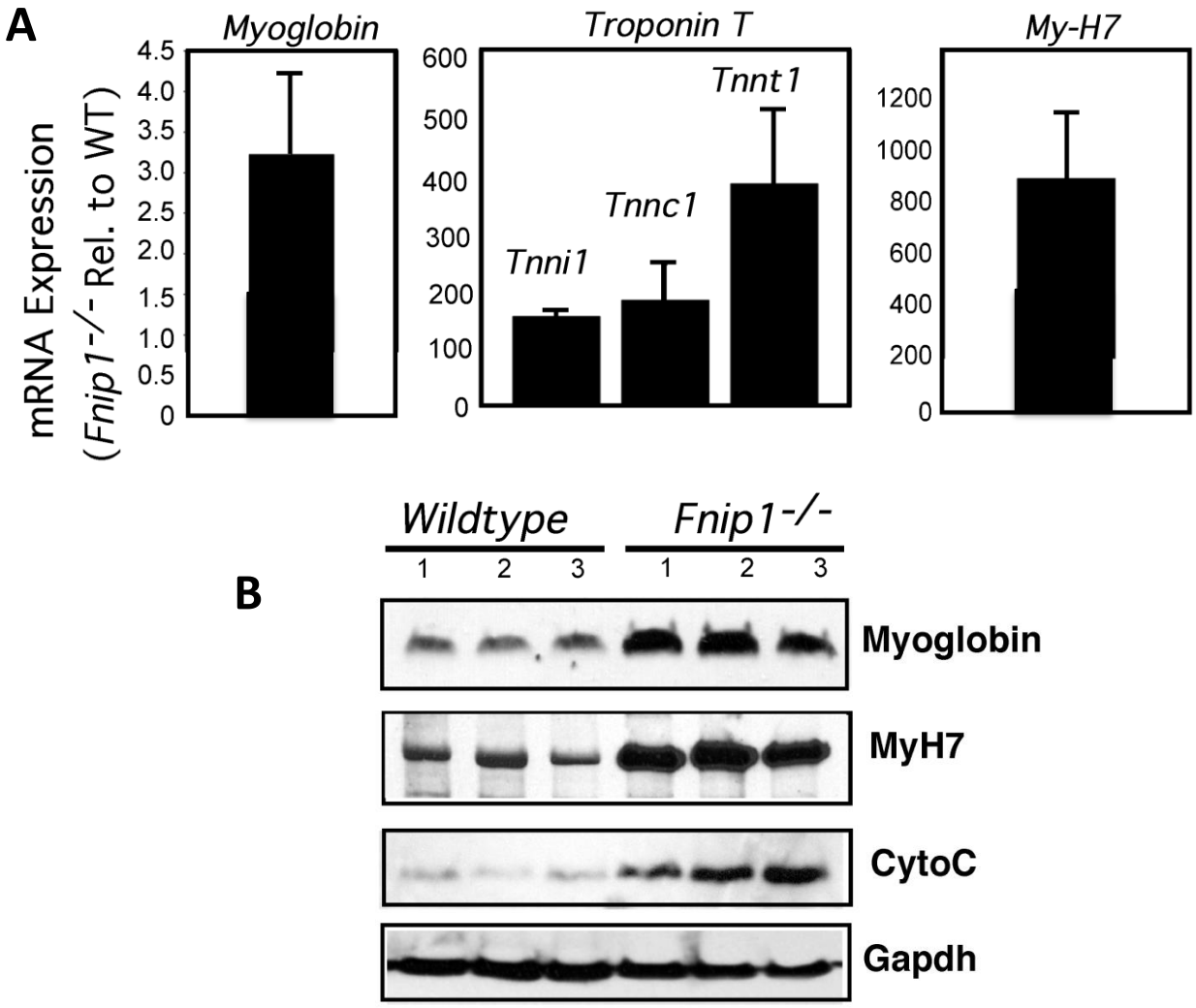

Figure 4. Fnip1 null skeletal muscle expresses increased levels of slow twitch specific genes and proteins.

(A) Gastrocnemius muscle RNA was extracted from 8-week old male mice. Gene expression was measured by quantitative real-time PCR (RT-PCR). Shown are the means +/- SEM from 4-6 mice/group. mRNA expression levels are shown as *Fnip1*$^{-/-}$ relative to Wt mice. **(B)** Immunoblotting of proteins characteristic of slow twitch muscle fibers. Proteins were isolated from gastrocnemius muscle. Shown are representative immunoblots showing 3 independent mice per group. Gapdh is shown as loading controls.

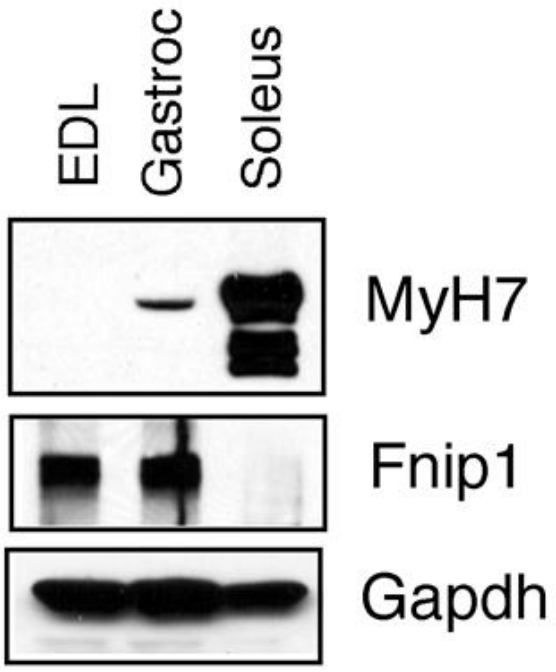

Figure 5. Fnip1 is normally expressed in Type II skeletal muscle.

Fnip1 protein is found predominantly in fast-twitch muscle fiber types. Western blot analysis was performed on protein extracted from the Extensor Digitalis Longus, Gastrocnemius, and Soleus muscles from an 8-week old male wild-type mouse.

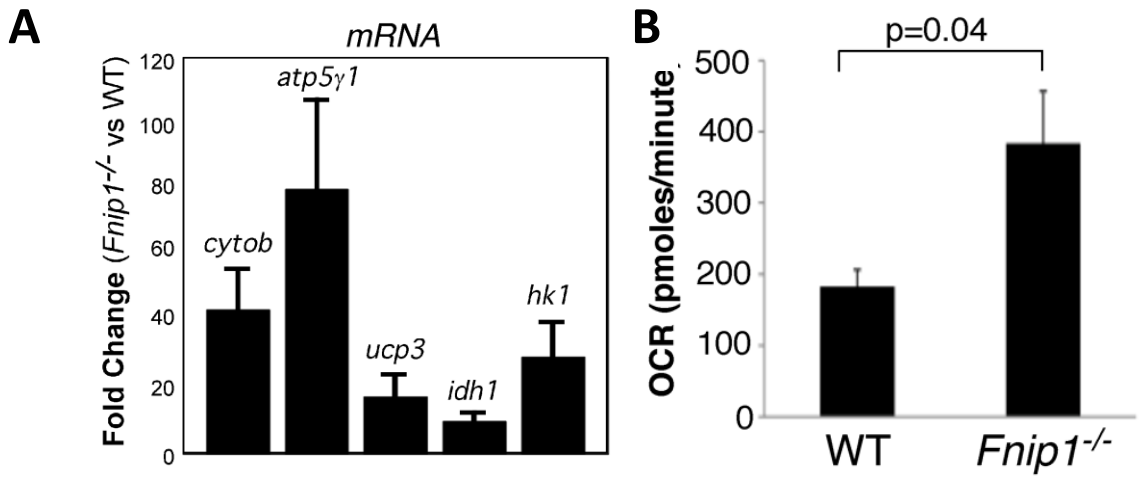

Figure 6. Disruption of Fnip1 increases the representation of highly oxidative fibers rich in mitochondria.

(A) Expression of mitochondrial specific genes were evaluated by RT-PCR on RNA extracted from the gastrocnemius muscle of *Fnip1*$^{-/-}$ mice and littermate controls. Shown are bar graphs from 3 mice per group. Mean +/- SEM are shown for 3-5 mice per group.

(B) Oxygen consumption rate (OCR) of adult myofibers isolated from the gastrocnemius muscle of *Fnip1*$^{-/-}$ mice and wild type littermates. Baseline OCR in plated myofibers was measured (n=3 mice per genotype). Myofibers within each genotype were combined and plated in 3-6 replicate wells/genotype. Error bars represent mean and SEM of 3 mice per group. Graph is representative of 3 independent experiments.

Sample Name	*Fnip1*$^{-/-}$ /WT	P-value:	KEGG Pathway
Proline	0.474	0.003	*Amino Acid*
Asparagine	1.815	0.043	*Amino Acid*
Glutamine	2.400	0.003	*Amino Acid*
Glutamic acid	1.615	0.031	*Amino Acid*
Pyroglutamic Acid	3.281	0.010	*Amino acids/Glu*
gamma-Aminobutyrate	3.061	0.011	*Amino Acid metabolism/Ala, Glu, Asp*
Citraconic Acid	1.835	0.002	*Amino Acid metabolism/Val, Leu, IL*
MethylSuccinate	1.761	0.046	*Amino Acid metabolism/Isoleucine*
Xanthine	1.962	0.015	*Nucleotide*
Hypoxanthine	2.614	0.016	*Nucleotide*
Adenine	1.658	0.028	*Nucleotide/Purine metabolism*
Alpha-Ketoglutaric Acid	2.793	0.015	*TCA Cycle*
Aconitate	1.852	0.005	*TCA Cycle*
Linolenic Acid	2.565	0.047	*Fatty acid metabolism*
Citrulline	2.514	0.032	*Urea Cycle*
L-Kynurenine	1.933	0.016	*Tryptophan Cycle*
Geranyl Pyrophosphate	3.28	0.010	*Ubiquinone and other terpenoid-quinone biosynthesis*
Niacinamide	1.847	0.002	*Vitamins*

Figure 7. Increases in amino acid, TCA cycle, and fatty acid metabolites in *Fnip1*$^{-/-}$ skeletal muscle.

Comparison of metabolite concentrations measured from samples of the gastrocnemius muscle isolated from age and sex matched *Fnip1*$^{-/-}$ mice and Wt controls. Results were normalized to tissue mass. Molecules which were present at significantly different concentrations were identified via mass spectrometry and categorized based on the Kyoto Encyclopedia of Genes and Genomes (KEGG) metabolic pathway classification system.

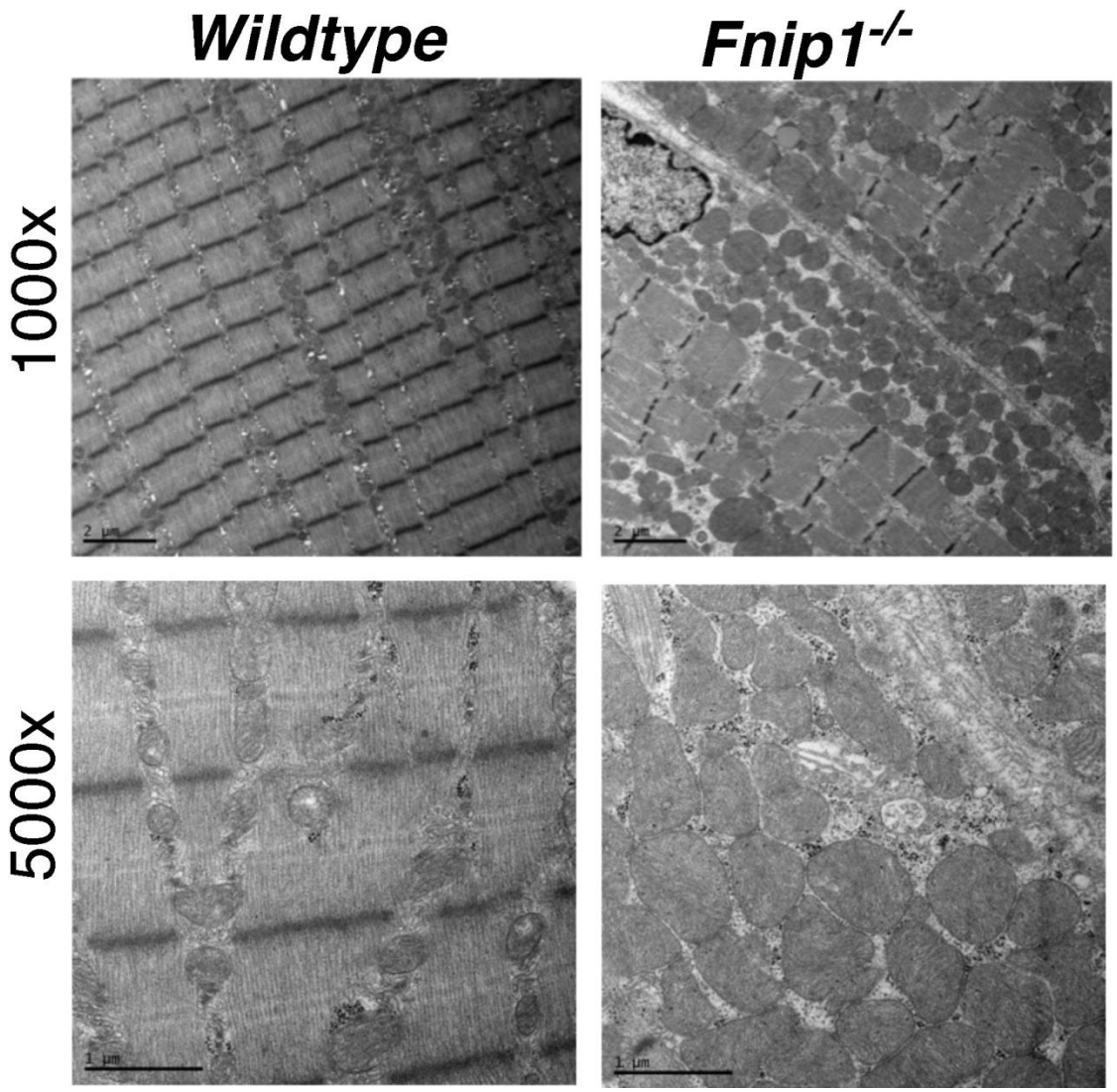

Figure 8. *Fnip1*$^{-/-}$ skeletal muscle contains increased mitochondrial mass.

Representative electron micrographs of gastrocnemius muscle taken from 8 week-old male mice. Shown are 1000X and 5000X magnified images.

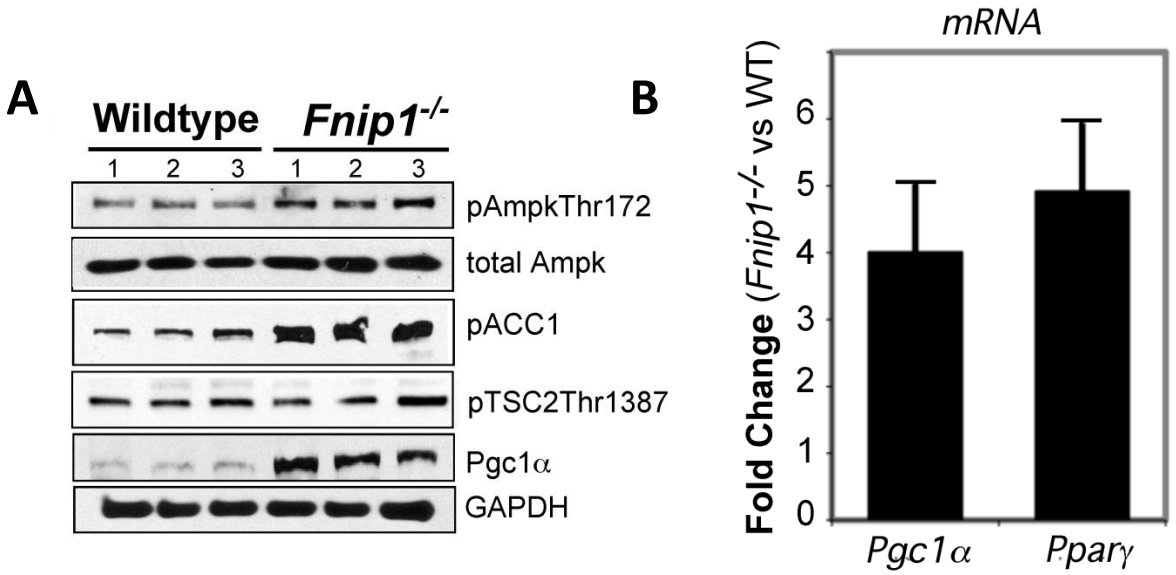

Figure 9. *Fnip1*$^{-/-}$ skeletal muscles exhibit hyperactivation of the AMPK/PGC1α pathway.

(A) Immunoblots were performed on protein lysate extracted from gastrocnemius muscles of age and sex-matched mice. Shown are representative immunoblots from 3 mice of each genotype. 1,2,3 represent individual mice of each genotype.

(B) Expression of PGC1α and PPARγ were determined via RT-PCR of RNA extracted from the gastrocnemius of age and sex-matched mice (n=6). Shown are bar graphs depicting the mean +/- SEM from 3 mice per group.

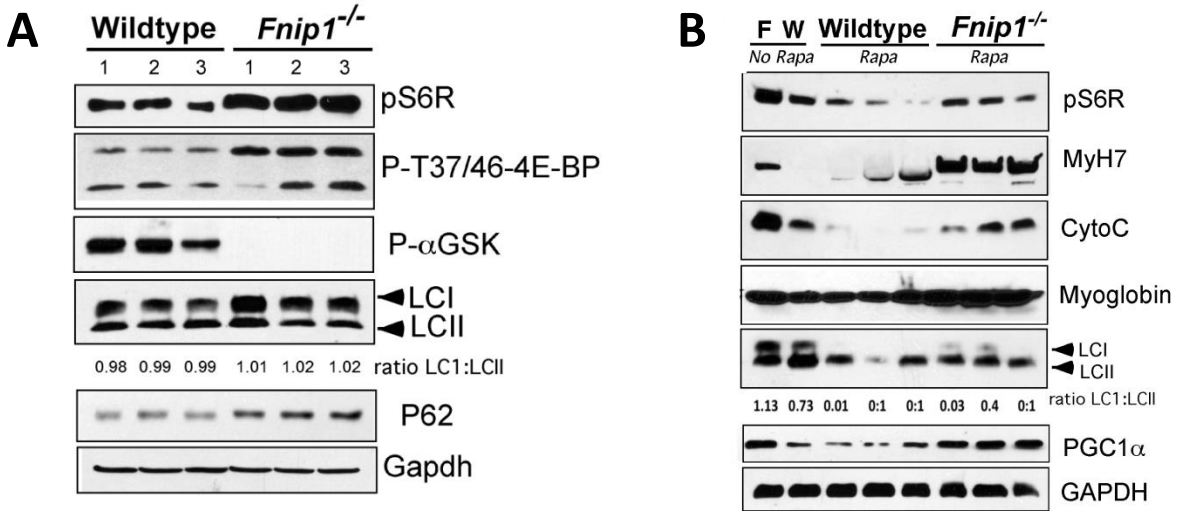

Figure 10. mTOR pathway is hyperactivated and autophagy is inhibited in Fnip1 null skeletal muscle.

(A) Immunoblots performed on protein lysate extracted from the gastrocnemius muscles of age and sex-matched mice. 1,2,3 represent individual mice of each genotype.

(B) Mice were fed either normal diet or rapamycin diet beginning in utero and extending until 4-5 weeks of age (n=5/group). Rapamycin inhibited mTOR and partially restored autophagy but failed to rescue fiber type specification. Shown are immunoblots derived from 3 mice per group. W=Wt controls, F=*Fnip1*$^{-/-}$ controls. Gapdh is shown as a protein loading control.

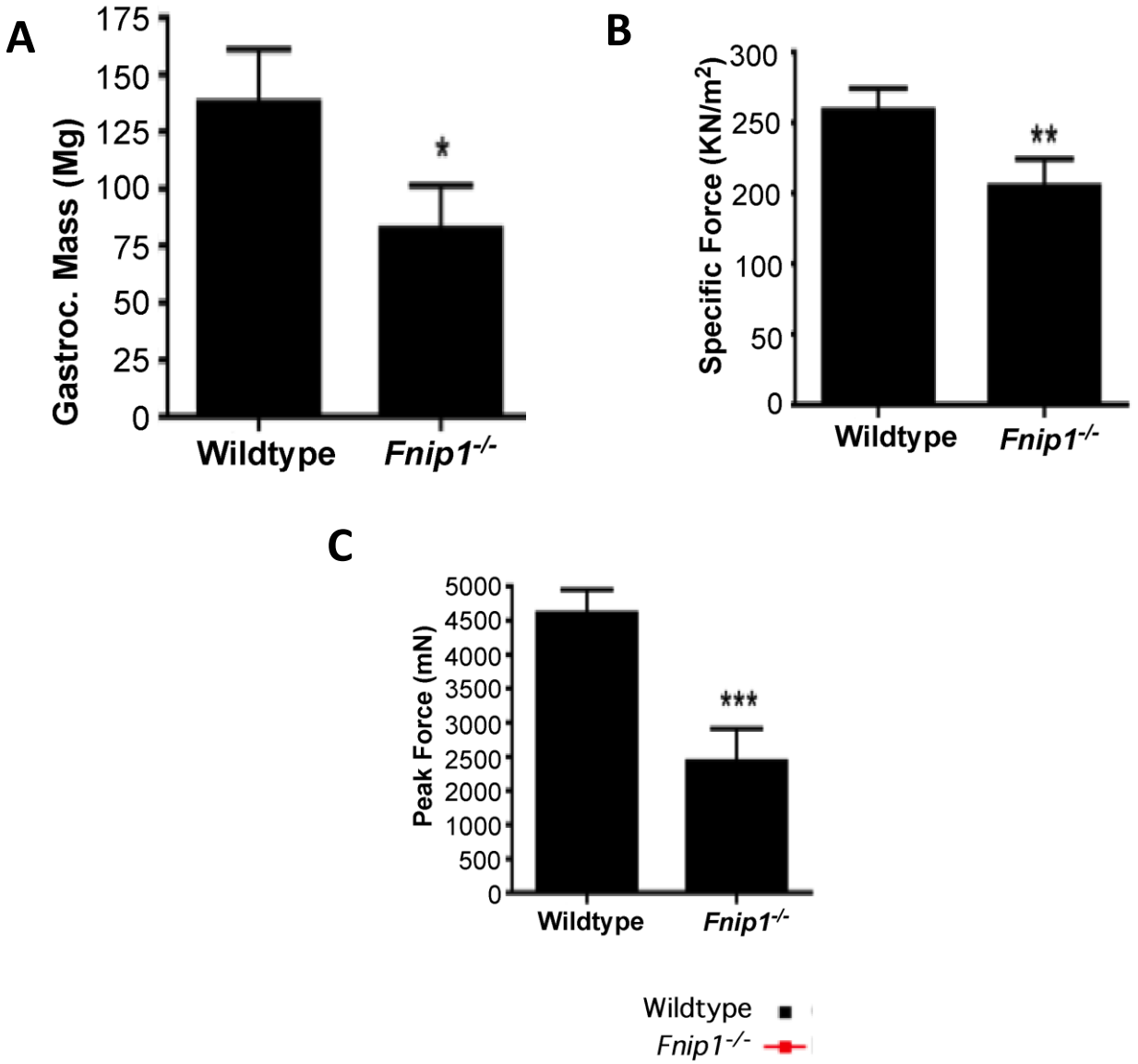

Figure 11. Fnip1$^{-/-}$ skeletal muscles are smaller and produce less force when compared to WT controls.

(A) Reduced mass of gastrocnemius muscle isolated from *Fnip1*$^{-/-}$ mice relative to Wt mice. Shown is the mean +/- SEM from 4 mice per group.

(B-C) *Fnip1*$^{-/-}$ mice produce reduced specific force (B) and peak force (C) relative to Wt mice. Contraction force measurements performed in situ on the gastrocnemius muscle of anesthetized 8-week old male *Fnip1*$^{-/-}$ and Wt mice in situ (n=4/group).

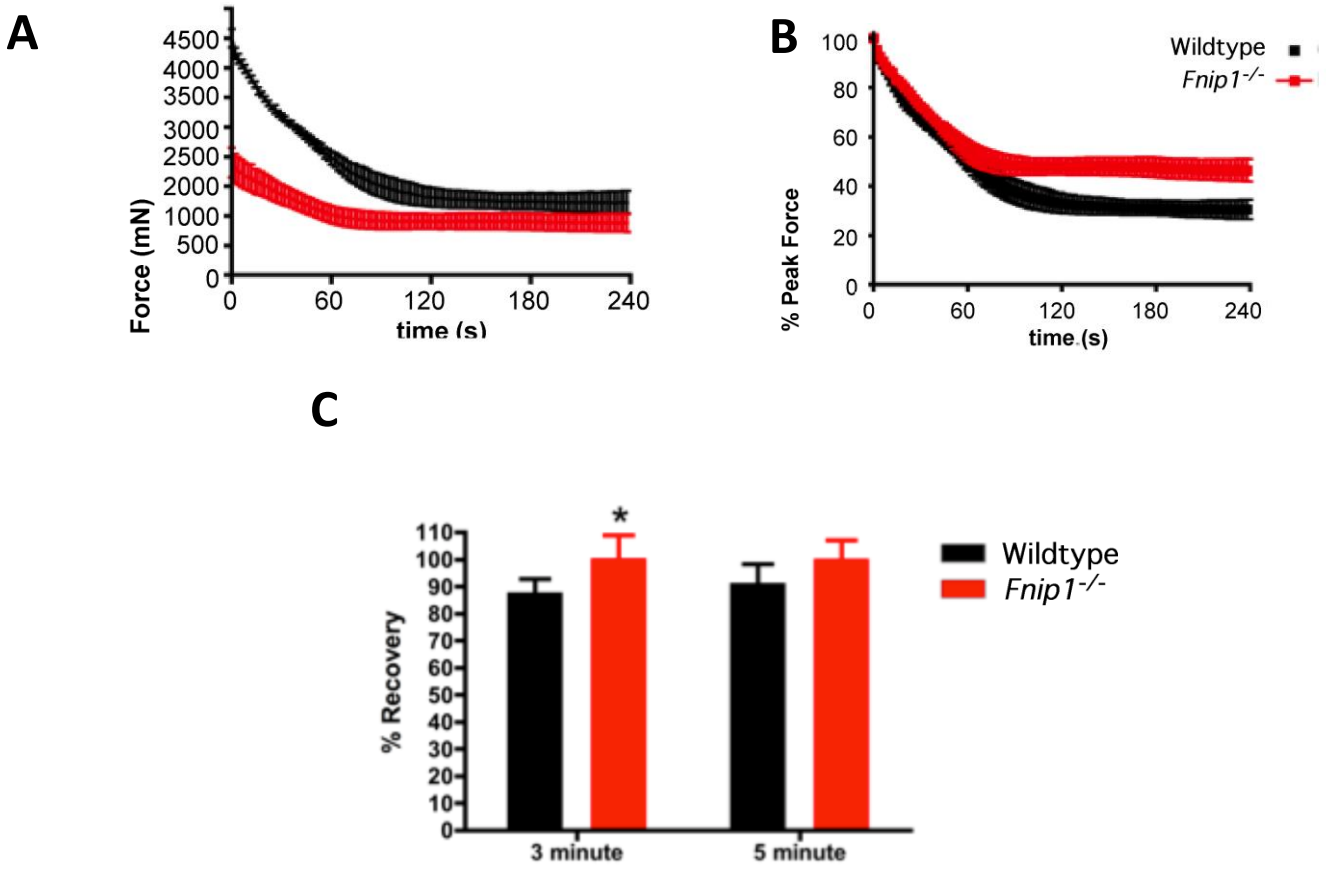

Figure 12. *Fnip1* null skeletal muscles are more resistant to fatigue and display rapid post contraction recovery.

(A,B) *Fnip1*$^{-/-}$ mice exhibit decreased post-contraction refractory duration relative to WT mice. The isolated muscle was stimulated to contract every 2 seconds for a total of 4 minutes. Subsequent to repeated contraction muscle was allowed to rest for a period of three minutes, directly followed by a single stimulation and measurement of the resulting recovery force. Red bar = *Fnip1*$^{-/-}$(n=4); Black bar= WT control (n=4). This protocol was repeated at an interval of 5 minutes. **(C)** Improved percent post-contraction recovery following disruption of Fnip1. Shown are the mean and SEM from 4 mice per group. *p<0.05. **p<0.01. ***<0.005.

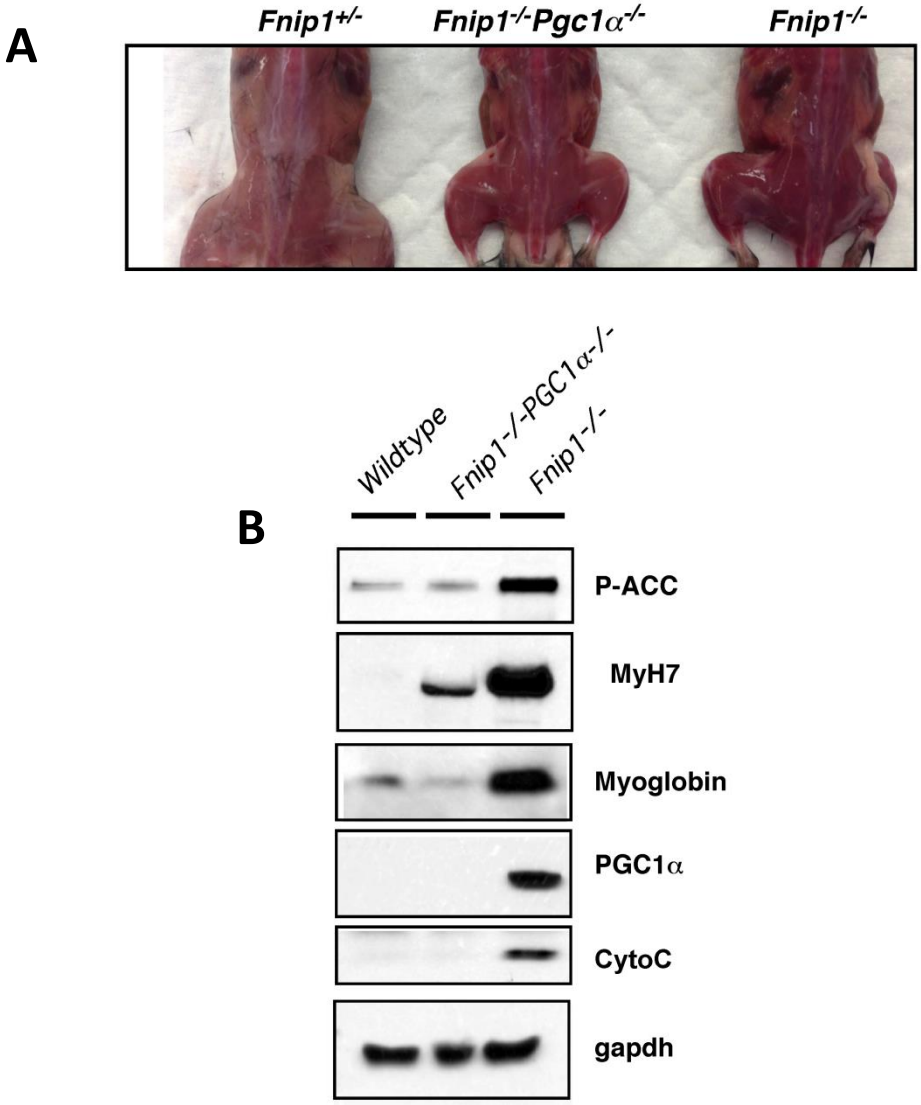

Figure 13. Disruption of PGC1α restores normal muscle fiber representation in *Fnip1*$^{-/-}$ mice.

(A) *Fnip1*$^{-/-}$*PGC1α*$^{-/-}$ double knockout mice display an intermediate skeletal muscle coloration phenotype relative to WT and *Fnip1*$^{-/-}$ mice. Gross images taken shortly after euthanasia.

(B) Immunoblots performed on protein lysate extracted from the gastrocnemius muscles of age and sex-matched mice.

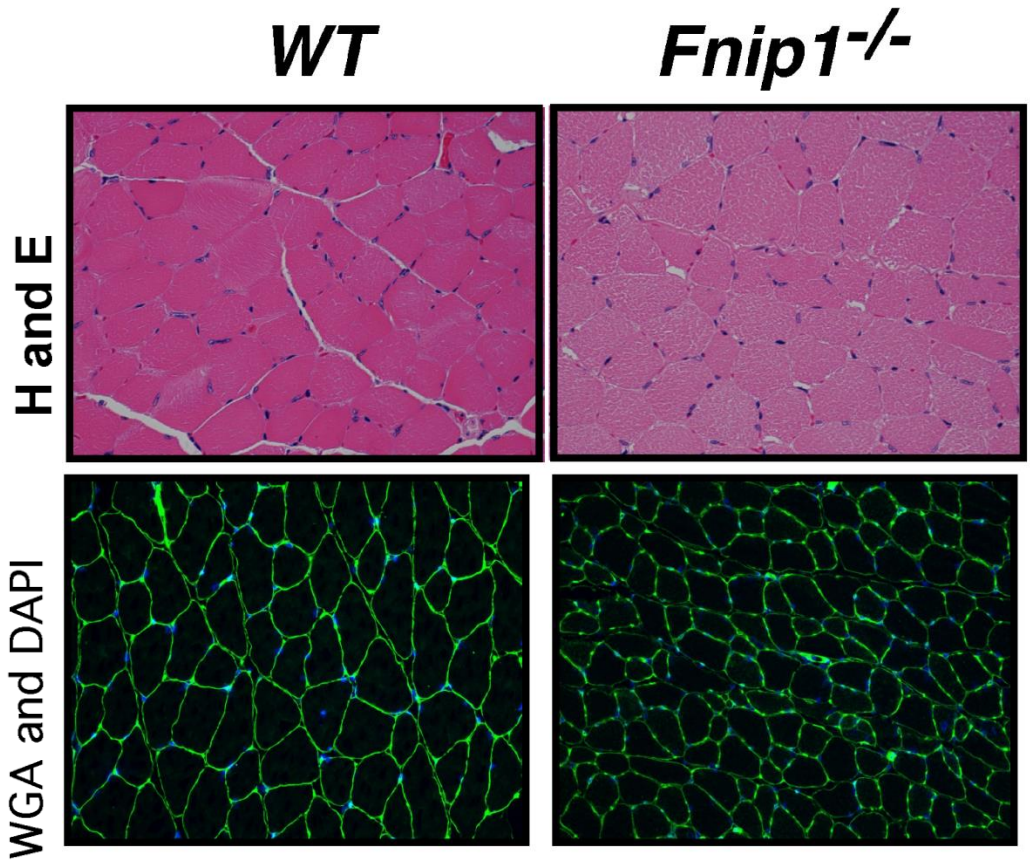

Figure 14. Fnip1 null skeletal muscles display normal cytoskeletal characteristics.

H&E staining was performed on formalin fixed *quadriceps* muscles (top) of *Fnip1* null and WT control mice (n=3/group). WGA plus DAPI staining, which assists in visualizing plasma membranes and nuclei, was performed on *gastrocnemius* muscles (bottom).

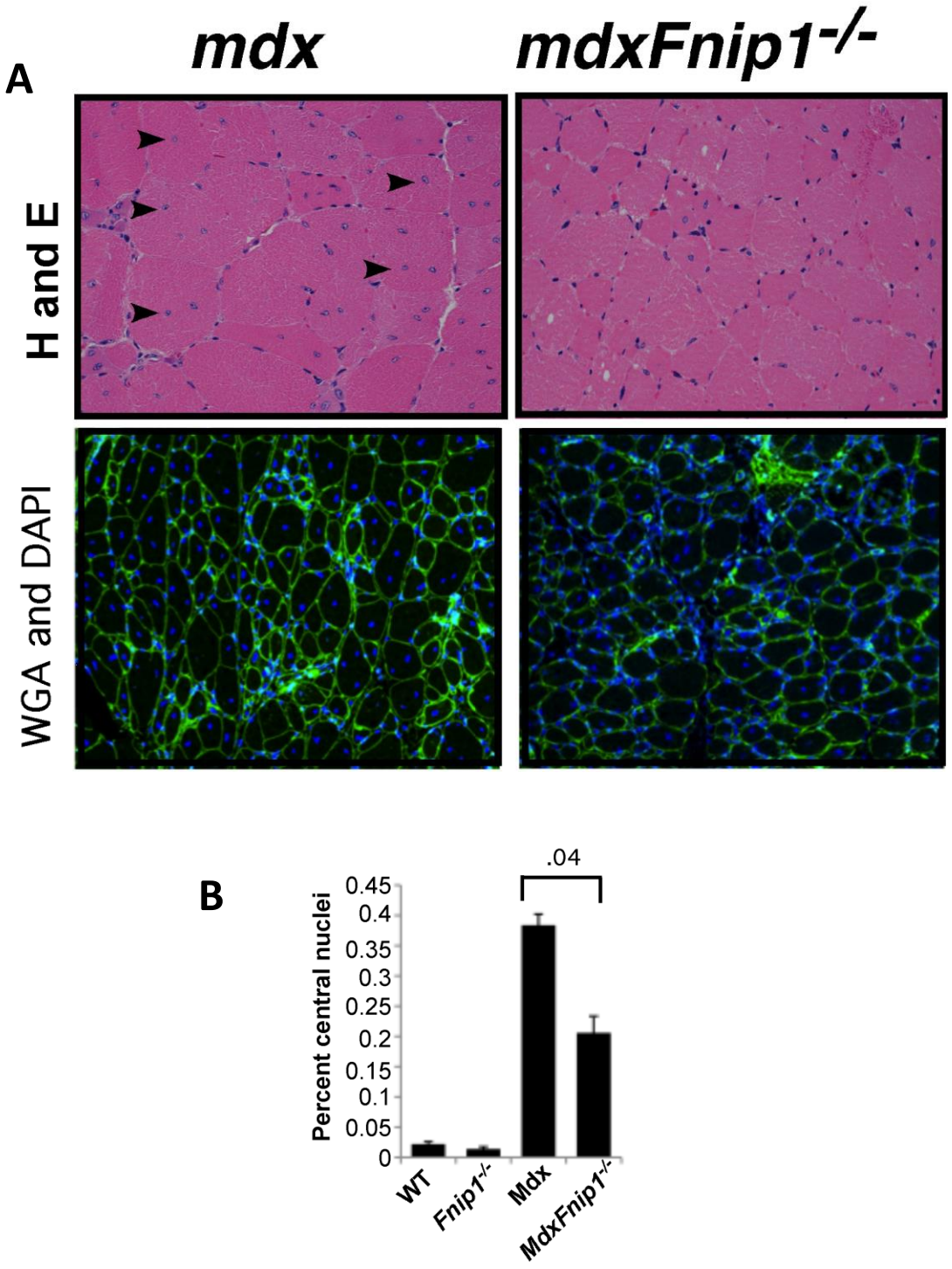

Figure 15. Disruption of Fnip1 significantly reduces muscle fiber damage and restores fiber integrity in Mdx muscular dystrophy mice.

(A) H&E staining was performed on formalin fixed *quadriceps* muscles (top), and WGA plus DAPI staining on gastrocnemius muscles (bottom), which assists in visualizing plasma membranes (Green) and nuclei (Blue) respectively. Black arrows mark centralized nuclei.

(B) Nuclei were counted in 10 random fields per genotype (n=3/genotype) in a blinded fashion.

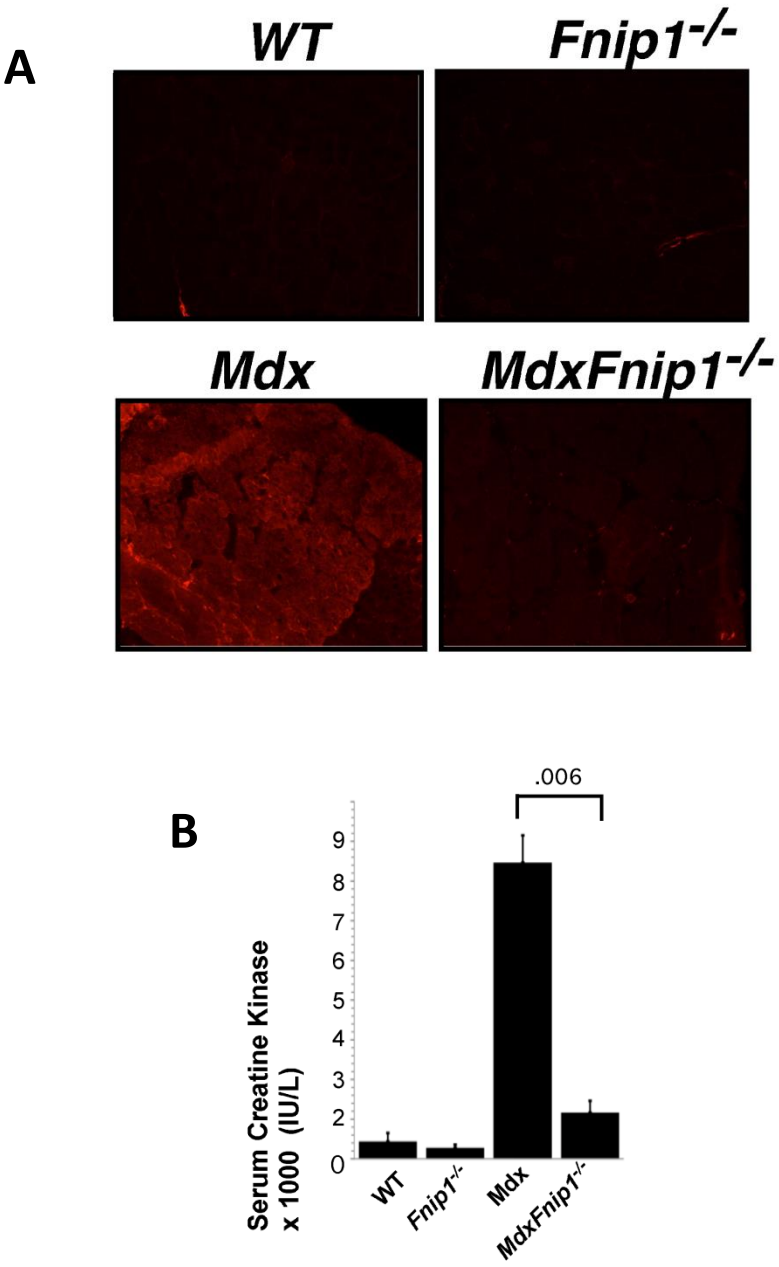

Figure 16. Disruption of Fnip1 significantly prevents muscle fiber damage and restores muscle fiber integrity in Mdx muscular dystrophy mice.

(A) Loss of *Fnip1* expression significantly reduces extravasation of Evan's Blue Dye in Mdx mice 20 hours post-injection. Shown are representative images of cross sections of gastrocnemius muscle harvested from mice of the listed genotypes. Dye leakage was analyzed by fluorescent microscopy.

(B) Inhibition of Fnip1 significantly reduces serum creatine kinase levels in Mdx mice. Creatine kinase levels were determined by colorimetric assay. Bar graphs represent the mean+/- SEM of 3 mice per genotype.

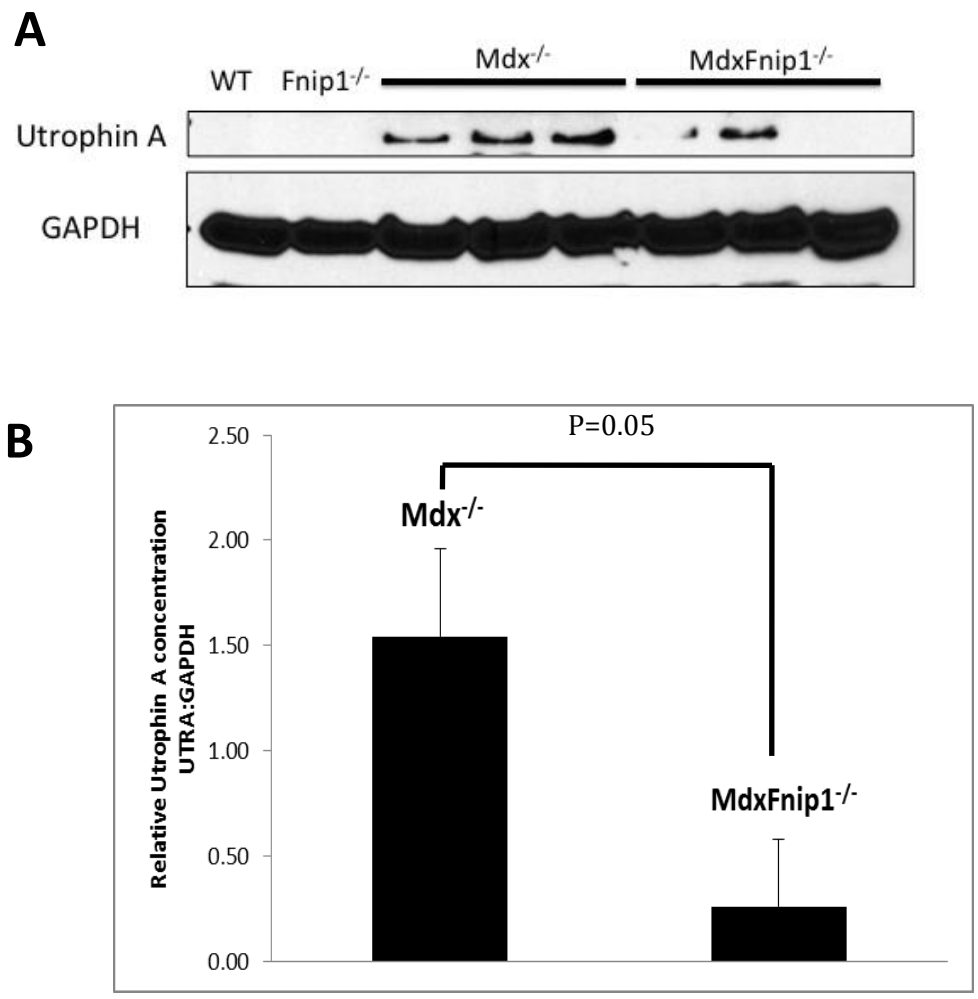

Figure 17. *Fnip1* null rescue of mdx skeletal muscle phenotype occurs independently of Utrophin A expression.

(A) Immunoblots performed on protein lysate extracted from the gastrocnemius muscles of age and sex-matched mice (n=3 mice/genotype). Image was analyzed using ImageJ (http://imagej.nih.gov/ij/). Results represent Utrophin A signal normalized to loading control (GAPDH).

(B) Shown are mean +/- SEM relative Utrophin A concentration. P-values are shown.

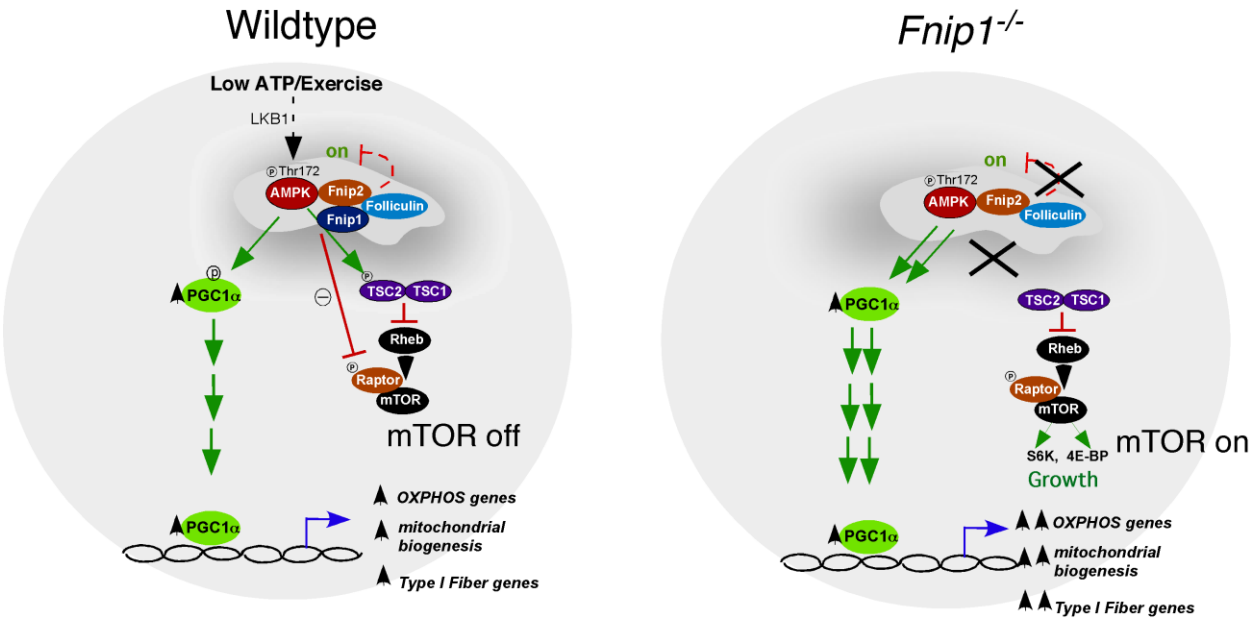

Figure 18. Model of Fnip1 functions in skeletal muscle.

(*Left*). Fnip1 interacts with AMPK, Fnip2, and Folliculin. Under conditions of low ATP/high AMP or exercise, AMPK is phosphorylated at threonine 172 by LKB kinase. Activated AMPK stimulates energy production in part by phosphorylating and increasing transcription of PGC1α, resulting in increased PGC1α protein. PGC1α then stimulates transcription of essential genes involved in oxidative phosphorylation (OXPHOS), mitochondrial biogenesis, and type I fiber type specification including PPARγ, PPARα, estrogen receptor-related α (ERRa), FoxO1, hepatocyte nuclear factor 4α (HNF4α), and nuclear respiratory factor 1 (NRF1). Activated AMPK concurrently inhibits energy consumption mediated by mTOR by phosphorylating and activating the Rheb GTPase inhibitor TSC2, and by phosphorylating and activating the mTOR activator Raptor. Fnip1 is normally required for AMPK to efficiently inhibit mTOR, and to turn off AMPK activation in response to low energy. (*Right*) In the absence of Fnip1, AMPK is hyperactivated in response to energy or nutrient deprivation, resulting in increased PGC1α expression, increased mitochondrial biogenesis, and type I fiber type switch. AMPK also fails to efficiently inhibit mTOR, resulting in increased mTOR mediated nutrient consumption, which further feeds back to activate AMPK.

References

1. Booth FW, Thomason DB: **Molecular and cellular adaptation of muscle in response to exercise: perspectives of various models.** *Physiol Rev* 1991, **71:**541-585.
2. Jarvis JC, Mokrusch T, Kwende MM, Sutherland H, Salmons S: **Fast-to-slow transformation in stimulated rat muscle.** *Muscle Nerve* 1996, **19:**1469-1475.
3. Pette D: **Training effects on the contractile apparatus.** *Acta Physiol Scand* 1998, **162:**367-376.
4. Narkar VA, Downes M, Yu RT, Embler E, Wang YX, Banayo E, Mihaylova MM, Nelson MC, Zou Y, Juguilon H, et al: **AMPK and PPARdelta agonists are exercise mimetics.** *Cell* 2008, **134:**405-415.
5. Hardie DG: **Energy sensing by the AMP-activated protein kinase and its effects on muscle metabolism.** *Proc Nutr Soc* 2011, **70:**92-99.
6. Gowans GJ, Hardie DG: **AMPK: a cellular energy sensor primarily regulated by AMP.** *Biochem Soc Trans* 2014, **42:**71-75.
7. O'Neill HM, Maarbjerg SJ, Crane JD, Jeppesen J, Jorgensen SB, Schertzer JD, Shyroka O, Kiens B, van Denderen BJ, Tarnopolsky MA, et al: **AMP-activated protein kinase (AMPK) beta1beta2 muscle null mice reveal an essential role for AMPK in maintaining mitochondrial content and glucose uptake during exercise.** *Proc Natl Acad Sci U S A* 2011, **108:**16092-16097.
8. Zong H, Ren JM, Young LH, Pypaert M, Mu J, Birnbaum MJ, Shulman GI: **AMP kinase is required for mitochondrial biogenesis in skeletal muscle in response to chronic energy deprivation.** *Proc Natl Acad Sci U S A* 2002, **99:**15983-15987.
9. Barnes BR, Marklund S, Steiler TL, Walter M, Hjalm G, Amarger V, Mahlapuu M, Leng Y, Johansson C, Galuska D, et al: **The 5'-AMP-activated protein kinase gamma3 isoform has a key role in carbohydrate and lipid metabolism in glycolytic skeletal muscle.** *J Biol Chem* 2004, **279:**38441-38447.
10. Garcia-Roves PM, Osler ME, Holmstrom MH, Zierath JR: **Gain-of-function R225Q mutation in AMP-activated protein kinase gamma3 subunit increases mitochondrial biogenesis in glycolytic skeletal muscle.** *J Biol Chem* 2008, **283:**35724-35734.
11. Wu H, Kanatous SB, Thurmond FA, Gallardo T, Isotani E, Bassel-Duby R, Williams RS: **Regulation of mitochondrial biogenesis in skeletal muscle by CaMK.** *Science* 2002, **296:**349-352.
12. Naya FJ, Mercer B, Shelton J, Richardson JA, Williams RS, Olson EN: **Stimulation of slow skeletal muscle fiber gene expression by calcineurin in vivo.** *J Biol Chem* 2000, **275:**4545-4548.
13. Kramerova I, Kudryashova E, Ermolova N, Saenz A, Jaka O, Lopez de Munain A, Spencer MJ: **Impaired calcium calmodulin kinase signaling and muscle adaptation response in the absence of calpain 3.** *Hum Mol Genet* 2012, **21:**3193-3204.
14. Parsons SA, Wilkins BJ, Bueno OF, Molkentin JD: **Altered skeletal muscle phenotypes in calcineurin Aalpha and Abeta gene-targeted mice.** *Mol Cell Biol* 2003, **23:**4331-4343.
15. Zechner C, Lai L, Zechner JF, Geng T, Yan Z, Rumsey JW, Collia D, Chen Z, Wozniak DF, Leone TC, Kelly DP: **Total skeletal muscle PGC-1 deficiency uncouples**

mitochondrial derangements from fiber type determination and insulin sensitivity. *Cell Metab* 2010, **12:**633-642.
16. Rowe GC, Patten IS, Zsengeller ZK, El-Khoury R, Okutsu M, Bampoh S, Koulisis N, Farrell C, Hirshman MF, Yan Z, et al: **Disconnecting mitochondrial content from respiratory chain capacity in PGC-1-deficient skeletal muscle.** *Cell Rep* 2013, **3:**1449-1456.
17. Handschin C, Kobayashi YM, Chin S, Seale P, Campbell KP, Spiegelman BM: **PGC-1alpha regulates the neuromuscular junction program and ameliorates Duchenne muscular dystrophy.** *Genes Dev* 2007, **21:**770-783.
18. Lin J, Wu H, Tarr PT, Zhang CY, Wu Z, Boss O, Michael LF, Puigserver P, Isotani E, Olson EN, et al: **Transcriptional co-activator PGC-1 alpha drives the formation of slow-twitch muscle fibres.** *Nature* 2002, **418:**797-801.
19. Jager S, Handschin C, St-Pierre J, Spiegelman BM: **AMP-activated protein kinase (AMPK) action in skeletal muscle via direct phosphorylation of PGC-1alpha.** *Proc Natl Acad Sci U S A* 2007, **104:**12017-12022.
20. Appleby MW, Ramsdell F: **A forward-genetic approach for analysis of the immune system.** *Nat Rev Immunol* 2003, **3:**463-471.
21. Park H, Staehling K, Tsang M, Appleby MW, Brunkow ME, Margineantu D, Hockenbery DM, Habib T, Liggitt HD, Carlson G, Iritani BM: **Disruption of Fnip1 Reveals a Metabolic Checkpoint Controlling B Lymphocyte Development.** *Immunity* 2012.
22. Baba M, Hong SB, Sharma N, Warren MB, Nickerson ML, Iwamatsu A, Esposito D, Gillette WK, Hopkins RF, 3rd, Hartley JL, et al: **Folliculin encoded by the BHD gene interacts with a binding protein, FNIP1, and AMPK, and is involved in AMPK and mTOR signaling.** *Proc Natl Acad Sci U S A* 2006, **103:**15552-15557.
23. Hasumi H, Baba M, Hong SB, Hasumi Y, Huang Y, Yao M, Valera VA, Linehan WM, Schmidt LS: **Identification and characterization of a novel folliculin-interacting protein FNIP2.** *Gene* 2008, **415:**60-67.
24. Takagi Y, Kobayashi T, Shiono M, Wang L, Piao X, Sun G, Zhang D, Abe M, Hagiwara Y, Takahashi K, Hino O: **Interaction of folliculin (Birt-Hogg-Dube gene product) with a novel Fnip1-like (FnipL/Fnip2) protein.** *Oncogene* 2008, **27:**5339-5347.
25. Linehan WM, Pinto PA, Bratslavsky G, Pfaffenroth E, Merino M, Vocke CD, Toro JR, Bottaro D, Neckers L, Schmidt LS, Srinivasan R: **Hereditary kidney cancer: unique opportunity for disease-based therapy.** *Cancer* 2009, **115:**2252-2261.
26. Lin J, Wu PH, Tarr PT, Lindenberg KS, St-Pierre J, Zhang CY, Mootha VK, Jager S, Vianna CR, Reznick RM, et al: **Defects in adaptive energy metabolism with CNS-linked hyperactivity in PGC-1alpha null mice.** *Cell* 2004, **119:**121-135.
27. Bulfield G, Siller WG, Wight PA, Moore KJ: **X chromosome-linked muscular dystrophy (mdx) in the mouse.** *Proc Natl Acad Sci U S A* 1984, **81:**1189-1192.
28. Ruegg UT: **Pharmacological prospects in the treatment of Duchenne muscular dystrophy.** *Curr Opin Neurol* 2013, **26:**577-584.
29. Koenig M, Hoffman EP, Bertelson CJ, Monaco AP, Feener C, Kunkel LM: **Complete cloning of the Duchenne muscular dystrophy (DMD) cDNA and preliminary genomic organization of the DMD gene in normal and affected individuals.** *Cell* 1987, **50:**509-517.
30. Hoffman EP, Brown RH, Jr., Kunkel LM: **Dystrophin: the protein product of the Duchenne muscular dystrophy locus.** *Cell* 1987, **51:**919-928.

31. Monaco AP, Neve RL, Colletti-Feener C, Bertelson CJ, Kurnit DM, Kunkel LM: **Isolation of candidate cDNAs for portions of the Duchenne muscular dystrophy gene.** *Nature* 1986, **323:**646-650.
32. Stuart CA, McCurry MP, Marino A, South MA, Howell ME, Layne AS, Ramsey MW, Stone MH: **Slow-twitch fiber proportion in skeletal muscle correlates with insulin responsiveness.** *J Clin Endocrinol Metab* 2013, **98:**2027-2036.
33. Hambrecht R, Fiehn E, Yu J, Niebauer J, Weigl C, Hilbrich L, Adams V, Riede U, Schuler G: **Effects of endurance training on mitochondrial ultrastructure and fiber type distribution in skeletal muscle of patients with stable chronic heart failure.** *J Am Coll Cardiol* 1997, **29:**1067-1073.
34. Arany Z, Lebrasseur N, Morris C, Smith E, Yang W, Ma Y, Chin S, Spiegelman BM: **The transcriptional coactivator PGC-1beta drives the formation of oxidative type IIX fibers in skeletal muscle.** *Cell Metab* 2007, **5:**35-46.
35. Rockl KS, Hirshman MF, Brandauer J, Fujii N, Witters LA, Goodyear LJ: **Skeletal muscle adaptation to exercise training: AMP-activated protein kinase mediates muscle fiber type shift.** *Diabetes* 2007, **56:**2062-2069.
36. Mu J, Brozinick JT, Jr., Valladares O, Bucan M, Birnbaum MJ: **A role for AMP-activated protein kinase in contraction- and hypoxia-regulated glucose transport in skeletal muscle.** *Mol Cell* 2001, **7:**1085-1094.
37. Reznick RM, Zong H, Li J, Morino K, Moore IK, Yu HJ, Liu ZX, Dong J, Mustard KJ, Hawley SA, et al: **Aging-associated reductions in AMP-activated protein kinase activity and mitochondrial biogenesis.** *Cell Metab* 2007, **5:**151-156.
38. Jorgensen SB, Treebak JT, Viollet B, Schjerling P, Vaulont S, Wojtaszewski JF, Richter EA: **Role of AMPKalpha2 in basal, training-, and AICAR-induced GLUT4, hexokinase II, and mitochondrial protein expression in mouse muscle.** *Am J Physiol Endocrinol Metab* 2007, **292:**E331-339.
39. Thomson DM, Porter BB, Tall JH, Kim HJ, Barrow JR, Winder WW: **Skeletal muscle and heart LKB1 deficiency causes decreased voluntary running and reduced muscle mitochondrial marker enzyme expression in mice.** *Am J Physiol Endocrinol Metab* 2007, **292:**E196-202.
40. Inoki K, Zhu T, Guan KL: **TSC2 mediates cellular energy response to control cell growth and survival.** *Cell* 2003, **115:**577-590.
41. Gwinn DM, Shackelford DB, Egan DF, Mihaylova MM, Mery A, Vasquez DS, Turk BE, Shaw RJ: **AMPK phosphorylation of raptor mediates a metabolic checkpoint.** *Mol Cell* 2008, **30:**214-226.
42. Hsu PP, Kang SA, Rameseder J, Zhang Y, Ottina KA, Lim D, Peterson TR, Choi Y, Gray NS, Yaffe MB, et al: **The mTOR-regulated phosphoproteome reveals a mechanism of mTORC1-mediated inhibition of growth factor signaling.** *Science* 2011, **332:**1317-1322.
43. Mizushima N, Yoshimori T, Levine B: **Methods in mammalian autophagy research.** *Cell* 2010, **140:**313-326.
44. Cunningham JT, Rodgers JT, Arlow DH, Vazquez F, Mootha VK, Puigserver P: **mTOR controls mitochondrial oxidative function through a YY1-PGC-1alpha transcriptional complex.** *Nature* 2007, **450:**736-740.
45. Rowe GC, Safdar A, Arany Z: **Running forward: new frontiers in endurance exercise biology.** *Circulation* 2014, **129:**798-810.
46. Handschin C, Chin S, Li P, Liu F, Maratos-Flier E, Lebrasseur NK, Yan Z, Spiegelman BM: **Skeletal muscle fiber-type switching, exercise intolerance, and myopathy**

in PGC-1alpha muscle-specific knock-out animals. *J Biol Chem* 2007, **282:**30014-30021.
47. Hasumi H, Baba M, Hasumi Y, Huang Y, Oh H, Hughes RM, Klein ME, Takikita S, Nagashima K, Schmidt LS, Linehan WM: **Regulation of mitochondrial oxidative metabolism by tumor suppressor FLCN.** *J Natl Cancer Inst* 2012, **104:**1750-1764.
48. Katsetos CD, Koutzaki S, Melvin JJ: **Mitochondrial dysfunction in neuromuscular disorders.** *Semin Pediatr Neurol* 2013, **20:**202-215.
49. Webster C, Silberstein L, Hays AP, Blau HM: **Fast muscle fibers are preferentially affected in Duchenne muscular dystrophy.** *Cell* 1988, **52:**503-513.
50. Chan MC, Rowe GC, Raghuram S, Patten IS, Farrell C, Arany Z: **Post-natal induction of PGC-1alpha protects against severe muscle dystrophy independently of utrophin.** *Skelet Muscle* 2014, **4:**2.